CHALMERS

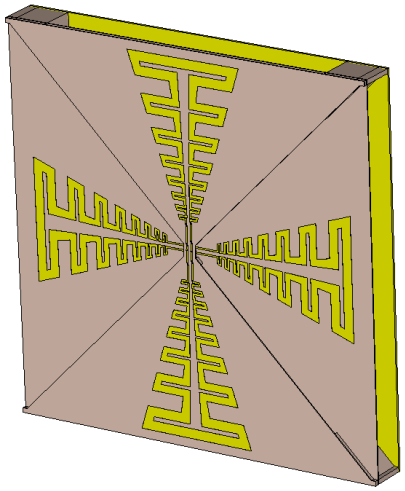

Design of a Planar Eleven Antenna as Wideband MIMO Micro-base Station Antenna with Genetic Algorithm

Thesis for the Master Degree of Communication Engineering

WENJIE YU

Division of Antenna Systems
Department of Signals and Systems
Chalmers University of Technology
Gothenburg, Sweden 2016

Master's Thesis 2016:

Master's thesis 2016:NN

Design of a Planar Eleven Antenna as Wideband MIMO Micro-base Station Antenna with Genetic Algorithm

WENJIE YU

CHALMERS
UNIVERSITY OF TECHNOLOGY

Division of Antenna Systems
Department of Signals and Systems
Chalmers University of Technology
Gothenburg, Sweden 2016

Design of a Planar Eleven Antenna as Wideband MIMO Micro-base Station Antenna with Genetic Algorithm

Supervisor: Associate professor Jian Yang, Division of Antenna Systems
Examiner: Professor Per-Simon Kildal, Division of Antenna Systems

Master's Thesis 2016:NN

Division of Antenna Systems
Department of Signals and Systems
Chalmers University of Technology
SE-412 96 Gothenburg

Typeset in LaTeX
Gothenburg, Sweden 2016

Abstract

Multi-input multi-output (MIMO) antennas operating over a wide frequency band are required in future wireless communication systems, such as in the 5G communication system.

The Eleven antenna is a dual-polarized ultra-wideband (UWB) antenna with a decade bandwidth. A new low-profile planar eleven antenna is designed as a wideband MIMO antenna for micro-base stations in future wireless communication systems. The design criterion is to minimize both the reflection coefficient and the ratio of the required average received power over the threshold for 95% of the total probability of detection (PoD) in the Rich Isotropic Multipath (RIMP) and random Line-of-Sight (RLOS) scenarios of both one-bit stream and two-bit stream. The design is performed via optimization with a genetic algorithm.

Acknowledgements

Firstly, I want to thank my examiner Professor Per-Simon Kildal for giving me the chance to do this master thesis project in the division of antenna systems. It is the most precious experience during the years at Chalmers University of Technology and also a invaluable experience in my life. It's a big pity that he passed away suddenly and unexpectedly before I finished the final data processing of this thesis.

I would like to thank my supervisor associate Professor Jian Yang for the guidance and help all the way from the beginning to the end of this thesis project. I was a student who only knew abstract theories and concepts from antenna books and only relied on formulas and derivation of equations to analyze antenna problems before doing this thesis project. I learned many engineer's thoughts and problem solving techniques for the real antenna design from doing the thesis project under Jian's supervision, which can never be obtained from books.

I would like to thank Dr. Ulf Calberg from Qamcom Research & Technology in Gothenburg for the help on the ViRMLab code for the simulation of the antenna. It's hard to imagine how much more time I would have to spend on this thesis project without his help. I learned a lot of ideas and tricks of programming from him.

I would like to thank PhD student in the division of antenna systems Sadegh Mansouri Moghaddam for detailed instruction on using the reverberation chamber for the radiation efficiency measurement, discussion on the probability of detection, help on the coverage pattern and a lot of other things that I'm not able to name one by one. I would like to thank PhD student Madeleine Kildal for the help on using the Bluetest software for the reverberation chamber.

Last but not least, I would like to thank my friends Weihua Wang and Junfei Tang at Chalmers University of Technology for accompany.

Wenjie Yu
Kunming, China, December 16, 2016

Contents

1

Introduction

1.1 History of Eleven antenna

Reflector antennas with wide bandwidth are required in the next-generation radio telescopes, such as the 1–10 GHz mid-band dish array of the SKA (Square Kilometer Array) project [1] and the 2–14 GHz VLBI2010 (Very Long Baseline Interferometry 2010) project [2].

The first Eleven feed, featured as a low-profile ultra-wideband (UWB) logarithmic-periodic array antenna with a constant beamwidth and a fixed phase center location, was developed in Chalmers University of Technology [3] ten years ago. Its basic configuration consists of pairs of half-wave dipoles (a pair of dipoles look like 11) cascaded and that's why it is named like so. The number of dipole pairs is selected according to the specification of the antenna bandwidth. A various kinds of Eleven antennas demonstrated good performance in radio telescope applications [4–9]. In addition to the applications for reflector antennas, the multi-port Eleven antenna has been studied for use in such as monopulse tracking systems [10] and UWB communication systems as a MIMO antenna [11, 12].

1.2 What's New in the present design

In this thesis, a new low-profile flat MIMO Eleven antenna for the applications in future 5G wireless communication systems is proposed. The flat Eleven MIMO antenna has a simple geometry and therefore a low manufacture cost.

The reasons that we choose the Eleven antenna as our candidate for investigation, analysis and design in this thesis project in applications of MIMO communication systems are that the Eleven antenna has a potential to cover large ultra-wideband and a good flexibility with number of ports. An Eleven antenna can be used as two-port, four-port and eight-port MIMO antennas with dual linear polarization or circular polar-

izations.

The design criteria takes into account both the reflection coefficient and the probability of detection under two edge environments, i.e. the rich isotropic multipath and the random Line-of-Sight for both one-bit stream and two-bit stream case.

This is the first time that the Eleven antenna is flatten and is designed for the measurement in the two edge environments.

1.3 Outline of this thesis

This thesis is organized as follows. Chapter 2 reviews the background theories, ranging from basic EM theory and antenna theory to optimization techniques and wireless communication theory, necessary for this antenna design project. Chapter 3 elaborates the detailed design and optimization procedure. Chapter 4 introduces two chambers, i.e. the anechoic chamber and the reverberation chamber, for the measurement and describes how the measurement is performed. Chapter 5 first shows the results from both the simulation and the measurement and then analyzes the results. Chapter 6 draws the conclusion based on the results.

2

Theory

This chapter reviews the basic theories involved in the thesis work, i.e., the basic electromagnetic field and wave theory originated from the Maxwell equations, antenna theory and figure of merits for designing antennas, basic theory of genetic algorithms for antenna optimization, OTA theory and technology, wireless communication theory and basic theories for a RF system.

2.1 Maxwell's Equations in Free Space and Propagation of EM wave

Maxwell's equations are a set of equations that describe how electric and magnetic fields are generated and altered by each other and by charges and currents. They are critical in understanding electromagnetic phenomenon. This simple review here only outlines the mathematical derivation from the Maxwell's equations to the wave equations while neglecting the detailed explanation from the physical point of view since the focus of the thesis work is antenna design. Classical electromagnetic theories are elaborated in a variety of books like [13], [14] and [15]. The first chapter of [16] gives a quite straightforward and useful summary of Maxwell's equations from the viewpoint of a microwave engineer and it's the main source of the electromagnetic theory reviewed in this section.

$$\begin{cases} \nabla \times \bar{E} = -\dfrac{\partial \bar{B}}{\partial t} - \bar{M} & \texttt{Faraday's Law} \quad (2.1a) \\ \nabla \times \bar{H} = \dfrac{\partial \bar{D}}{\partial t} + \bar{J} & \texttt{Ampere's Law} \quad (2.1b) \\ \nabla \cdot \bar{D} = \rho & \texttt{Gauss' Law} \quad (2.1c) \\ \nabla \cdot \bar{B} = 0 & \texttt{Gauss' Magnetism Law} \quad (2.1d) \end{cases}$$

The sinusoidal form of the electric and magnetic field is

$$\bar{E} = E_x cos(\omega t + \phi_x)\hat{\mathbf{x}} + E_y cos(\omega t + \phi_y)\hat{\mathbf{y}} + E_z cos(\omega t + \phi_z)\hat{\mathbf{z}} \tag{2.2}$$

$$\bar{H} = H_x cos(\omega t + \phi_x)\hat{\mathbf{x}} + H_y cos(\omega t + \phi_y)\hat{\mathbf{y}} + H_z cos(\omega t + \phi_z)\hat{\mathbf{z}} \tag{2.3}$$

where E_x, E_y, E_z, H_x, H_y, H_z are functions of the coordinates x,y,z.

The constitutive relations gives:

$$\bar{D} = \epsilon\bar{E} = \epsilon_o\bar{E} + \bar{P} \tag{2.4}$$

$$\bar{H} = \mu\bar{H} = \frac{1}{\mu_o}\bar{B} - \bar{M} \tag{2.5}$$

In an isotropic linear material, where $\bar{P}$ is proportional to $\bar{E}$, and $\bar{M}$ is proportional to $\bar{B}$, the constitutive relations are straightforward. For the sake of simplicity, we don't discuss complicated case such as non-isotropic or anti-isotropic materials. The polarization P and the magnetization M can be expressed as:

$$\bar{P} = \epsilon_o\chi_e\bar{E} \tag{2.6}$$

$$\bar{M} = \chi_m\bar{H} \tag{2.7}$$

where χ_e is the electric susceptibility and χ_m is the magnetic susceptibility.

Combining equations (2.4), (2.5), (2.6) and (2.7), it gives:

$$\bar{D} = \epsilon\bar{E} = \epsilon_o(1 + \chi_e)\bar{E} \tag{2.8}$$

$$\bar{B} = \mu\bar{H} = \mu_o(1 + \chi_m)\bar{H} \tag{2.9}$$

The phasor form and the sinusoidal form are connected by

$$\bar{E} = Re[\bar{\mathbf{E}}e^{j\omega t}] \tag{2.10}$$

$$\bar{H} = Re[\bar{\mathbf{H}}e^{j\omega t}] \tag{2.11}$$

where $\bar{\mathbf{E}}$ and $\bar{\mathbf{H}}$ are functions of the coordinates x,y,z.

The phasor form of Maxwell's equations is therefore as follows.

$$\begin{cases} \nabla \times \bar{\mathbf{E}} = -j\omega\bar{\mathbf{B}} - \bar{\mathbf{M}} & \text{(2.12a)} \\ \nabla \times \bar{\mathbf{H}} = j\omega\bar{\mathbf{D}} + \bar{\mathbf{J}} & \text{(2.12b)} \\ \nabla \cdot \bar{\mathbf{D}} = \boldsymbol{\rho} & \text{(2.12c)} \\ \nabla \cdot \bar{\mathbf{B}} = 0 & \text{(2.12d)} \end{cases}$$

where $\mathbf{J}$ is the conduction current density in the dielectric material with conductivity σ. The current density is

$$\bar{\mathbf{J}} = \sigma\bar{\mathbf{E}} \tag{2.13}$$

which is Ohm's law from a point view of electromagnetic field.

In a region with no charges ($\rho = 0$), no currents ($\sigma = 0$) and no magnetic susceptibility ($\chi_m = 0$) such as vacuum, the Maxwell's equations becomes:

$$\begin{cases} \nabla \times \bar{\mathbf{E}} = -j\omega\mu\bar{\mathbf{H}} & \text{(2.14a)} \\ \nabla \times \bar{\mathbf{H}} = j\omega\epsilon\bar{\mathbf{E}} & \text{(2.14b)} \\ \nabla \cdot \bar{\mathbf{E}} = 0 & \text{(2.14c)} \\ \nabla \cdot \bar{\mathbf{H}} = 0 & \text{(2.14d)} \end{cases}$$

Taking the curl operation ($\nabla\times$) on both sides of equation (2.14a) and (2.14b), it gives

$$\nabla \times (\nabla \times \bar{\mathbf{E}}) = \nabla(\nabla \cdot \bar{\mathbf{E}}) - \nabla^2\bar{\mathbf{E}} = -j\omega\mu\nabla \times \bar{\mathbf{H}} \tag{2.15}$$

$$\nabla \times (\nabla \times \bar{\mathbf{H}}) = \nabla(\nabla \cdot \bar{\mathbf{H}}) - \nabla^2\bar{\mathbf{H}} = j\omega\epsilon\nabla \times \bar{\mathbf{E}} \tag{2.16}$$

.

Plugging equation (2.14c) and (2.14d) into equation (2.15) and (2.16), then the wave equations or Helmholtz equations are obtained. That's how the Maxwell's equations predicts the existence and propagation of EM waves.

$$\begin{cases} \nabla^2\bar{\mathbf{E}} + \omega^2\mu\epsilon\bar{\mathbf{E}} = 0 & \text{(2.17a)} \\ \nabla^2\bar{\mathbf{H}} + \omega^2\mu\epsilon\bar{\mathbf{H}} = 0 & \text{(2.17b)} \end{cases}$$

2.2 General Review of RF Systems

This section simply reviews a few basic concepts of RF systems related to the antenna design in this thesis work. See [17], [16] and [18] for a deep understanding of microwave circuits and RF system.

2.2.1 Transmission line

The transmission line is a distributed parameter network, usually consisting of two parallel conductors. The length of the transmission line is on the order of several wavelength. It is an essential part in the RF systems and the components in the RF circuits, e.g. antenna, transistor, are connected with the transmission line.

2.2.2 Coaxial cable

The coaxial cable is a electrical cable composed of an inner conductor and an outer conductor. The space between the inner and outer conductor are filled with insulating material. The outer conductor is shielded by a protecting coat. The characteristic impedance of the coaxial cable can be tuned by selecting the diameters of the inner and outer conductor and the dielectric constant of the insulating layer. In this design project, coaxial cables with the characteristic impedance of 50Ω are used to connect the voltage source.

2.2.3 Scattering parameters

Scattering parameters, or S parameters for short, are the parameters relating the voltage waves incident on the ports to those reflected from the ports.

Consider an N-port network, the S parameter Sij is when port j is excited with incident voltage V_j^+ and reflected voltage V_i^- is measured at port i with all other ports terminated with their characteristic impedances

$$S_{ij} = \left.\frac{V_i^-}{V_j^+}\right|_{V_k^+=0 for k\neq j} \tag{2.18}$$

2.2.4 Block diagram of a whole RF system

The block diagram of the RF system in this antenna design project can be simplified as the following figure.

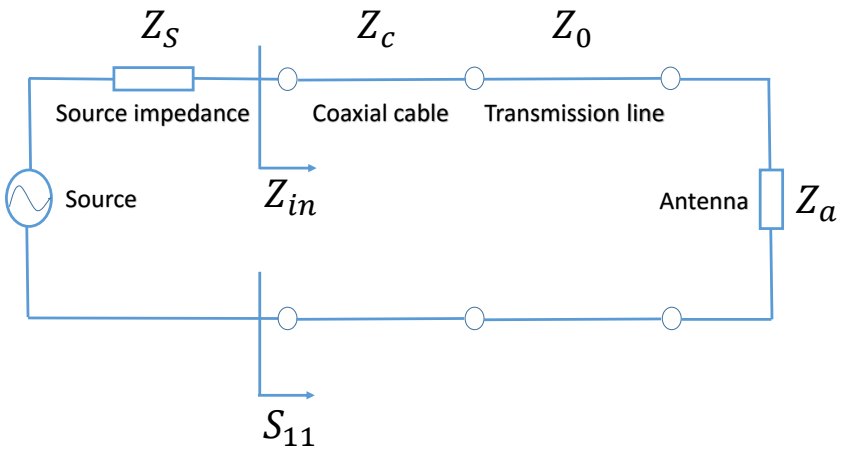

Figure 2.1: Block diagram of the RF system as a whole

The one-port S_{11} is calculated as

$$S_{11} = \frac{V_1^-}{V_1^+} = \frac{Z_{in} - Z_S}{Z_{in} + Z_S} \tag{2.19}$$

One important goal of this design project is to reduce the S_{11} so that it's in the acceptable range (around -10 dB). But the impedance of the antenna and the transmission line is varying when the design parameters of the antenna are changed. What's worse, there is no analytical formula for calculating the impedance. One way to solve this problem is to sweep all the design parameters that will influence the impedance one by one with very small steps. However, in this case the number of samples to simulated is quite large and thus the time needed for the simulation is very long. An alternative way, which is time-efficient, to solve this problem is to employ the so-called genetical algorithm for optimizing the design parameters. The detailed mechanism of genetic will be elaborated in section 2.4.

2.3 Basic Theories of Antennas

Wave equations (eq.(2.17a) and eq.(2.17b)) tell us that EM waves can propagate in the space. Antennas are the devices for the transmit and receive of EM waves. Antenna can be treated as a device, when working in a transmitter, that converts guided EM waves from the transmission line connected with it to plane waves in the space; when working in a receiver, that converts free space EM waves into guided waves and pass them to the transmission line connected with it.

2.3.1 General characterization of antennas

In this subsection, the common figures of merits that are generally used to characterize an antenna are described. The theories for antennas reviewed here are mainly taken from [19].

Radiation field and polarization of the antenna

At the observation point far away from the antenna the radiation field can be regarded as a propagating plane wave. The time-harmonic electric field (E-field) and magnetic field (H-field) of a plane wave propagating in positive z direction are described as

$$\mathbf{E} = \mathbf{E}_t e^{-jkz} = [E_x \hat{\mathbf{x}} + E_y \hat{\mathbf{y}}] e^{-jkz} \tag{2.20}$$

$$\mathbf{H} = \frac{1}{\eta} \hat{\mathbf{z}} \times \mathbf{E}_t e^{-jkz} = \frac{1}{\eta} [E_x \hat{\mathbf{x}} + E_y \hat{\mathbf{y}}] e^{-jkz} \tag{2.21}$$

where $\eta = 377\Omega$ is the wave impedance in free space,

$$k = \frac{2\pi}{\lambda} \tag{2.22}$$

is the wavenumber,

$$\lambda = \frac{v_p}{f} \tag{2.23}$$

is the wavelength, where v_p is the phase velocity of the wave. In the vacuum, $v_p = 299792458m/s$.

Polarization of an electromagnetic wave is defined as the orientation of the radiated electric field vector [18]. Define the desired polarization of the wave to be radiated or received by the antenna as the co-polar component and the wave orthogonal to co-polar component as the cross-polar component. The E-field can be expressed in terms of co-polar and cross-polar components as

$$\mathbf{E} = (E_{co}\,\hat{\mathbf{co}} + E_{xp}\,\hat{\mathbf{xp}})e^{-jkz} \tag{2.24}$$

where $\hat{\mathbf{co}}$ is the unit vector of co-polar component and $\hat{\mathbf{co}}$ for the cross-polar component. Eq.(2.20) is equivalent to eq.(2.24) just in a different form.

Far-field criterion and function

The surrounding space of an antenna can be divided into three parts, i.e. the reactive near-field region, the radiating near-field (Fresnell) region and the far-field (Fraunhofer) region (see Fig. 2.2). The field structure and characteristics are quite complicated and difficult to study in both the reactive near-field region and the radiating near-field region. In the far-field region, the shape of the radiation pattern is constant with respect to distance and radiated field is dominant, with the electric and the magnetic fields orthogonal to each other and in this region the propagation direction is the same as that of plane waves. So in the antenna design, it is always focused on the far-field characteristics.

The far-field criterion is satisfied when

$$r \geq \frac{2D^2}{\lambda} \tag{2.25}$$

where D is the largest diameter of the antenna, r is the distance from the antenna to the field point. The far-field region in Fig. 2.2 is the region where $r > r_2$.

The far-field at a point $\mathbf{r}$, direction of the field pointing from somewhere inside the antenna (the origin of the coordinate system) to the field location, is expressed, in spherical coordinate system, as

$$\mathbf{E}(r,\theta,\phi) = \frac{1}{r}e^{-jkr}\mathbf{G}(\theta,\phi) \tag{2.26}$$

where k is the wave number and $\mathbf{G}(\theta,\phi)$ is the far-field function. It's more convenient to describe the field of the antenna in spherical coordinate system than in orthogonal coordinate system.

$$\mathbf{G}(\theta,\phi) = G_\theta(\theta,\phi)\,\hat{\boldsymbol{\theta}} + G_\phi(\theta,\phi)\,\hat{\boldsymbol{\phi}} \tag{2.27}$$

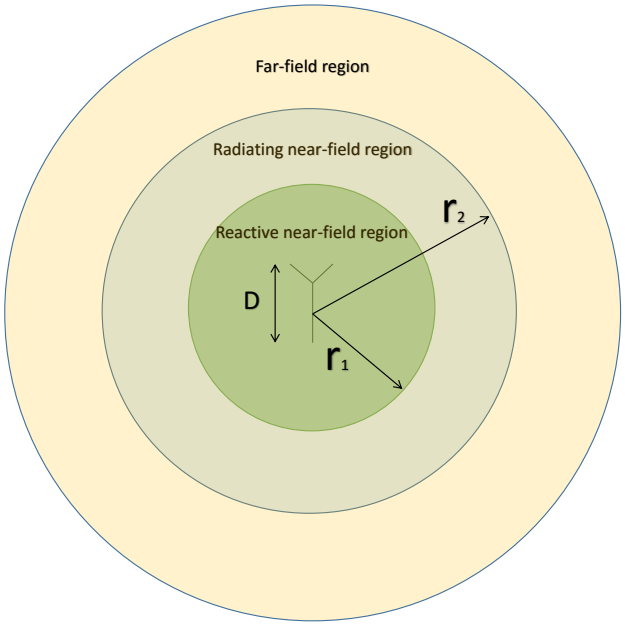

Figure 2.2: Field region of an antenna

where θ is the polar angle, ϕ is the azimuth angle. From vector calculus the transformation of coordinate system is according to the following formula

$$\hat{\boldsymbol{\theta}} = cos\theta cos\phi\hat{\mathbf{x}} + cos\theta sin\phi\hat{\mathbf{y}} - sin\theta\hat{\mathbf{z}} \tag{2.28}$$

$$\hat{\boldsymbol{\phi}} = -sin\phi\hat{\mathbf{x}} + cos\phi\hat{\mathbf{y}} \tag{2.29}$$

The far-field function Eq. 2.27 can be expressed alternatively in term of co-polar component and cross-polar component as

$$\mathbf{G}(\theta,\phi) = G_{co}(\theta,\phi)\,\hat{\mathbf{co}} + G_{xp}(\theta,\phi)\,\hat{\mathbf{xp}} \tag{2.30}$$

For linear y polarization the unit vectors of co-polar and cross-polar polarization are

$$\begin{cases} \hat{\mathbf{co}} = \hat{\mathbf{y}}' = sin\phi\,\hat{\boldsymbol{\theta}} + cos\phi\,\hat{\boldsymbol{\phi}} & \text{(2.31a)} \\ \hat{\mathbf{xp}} = \hat{\mathbf{x}}' = cos\phi\,\hat{\boldsymbol{\theta}} - sin\phi\,\hat{\boldsymbol{\phi}} & \text{(2.31b)} \end{cases}$$

Eq. (2.31a) and eq. (2.31b) is called Ludwig's third definition.

Then the expression of the far-field function of linear y polarization ($\mathbf{G}_y(\theta,\phi)$) and linear x polarization ($\mathbf{G}_x(\theta,\phi)$) are obtained in the spherical coordinate system as

$$\mathbf{G}_y(\theta,\phi) = [G_{co}(\theta,\phi)sin\phi + G_{xp}(\theta,\phi)cos\phi]\,\hat{\boldsymbol{\theta}} + [G_{co}(\theta,\phi)cos\phi - G_{xp}(\theta,\phi)sin\phi]\,\hat{\boldsymbol{\phi}} \tag{2.32}$$

$$\mathbf{G}_x(\theta,\phi) = [G_{co}(\theta,\phi)cos\phi + G_{xp}(\theta,\phi)sin\phi]\,\hat{\boldsymbol{\theta}} - [G_{co}(\theta,\phi)sin\phi - G_{xp}(\theta,\phi)cos\phi]\,\hat{\boldsymbol{\phi}} \quad (2.33)$$

If the mechanic structures of the antennas are rotationally symmetric, they are Bodies of Revolution (BOR). If a BOR antenna is excited by a short transverse current on the symmetry axis, it's called BOR_1 antenna. The reason for how it is named and the detailed derivation is in chapter 2 of [19]. The antenna designed in this thesis project is of BOR_1 type.

Reflection coefficient

The reflection coefficient (S_{11}) of an antenna is also an important criterion in the design. It is a measurement of how much power is reflected in the total power from the source. Usually we want the reflection coefficient as low as possible. In the optimization procedure, one main task is to reduce the reflection coefficient. The acceptable range of the reflection coefficient is $-10dB$ to $-5dB$.

Radiation pattern

The radiation pattern (or antenna pattern or far-field pattern) refers to the directional (angular) dependence of the strength of the radio waves from the antenna or other source [20]. In this design project, the desired radiation pattern is of the shape that can cover the window of spanning an angle of 120 degree in both the horizontal and the vertical direction of a sphere.

Directivity

Directivity is defined as the ratio of the power density in the direction where the antenna radiates most strongly to the power density of an ideal isotropic antenna, assuming the total radiated power is the same. It is a measure of how 'directional' an antenna's radiation pattern is.

Radiation efficiency

The total embedded radiation efficiency of element number i in an N-port system is

$$e_{rad} = 1 - \sum_{j=1}^{N} |S_{ji}|^2 \quad (2.34)$$

which takes into account the reflection in port i and the transmission from port i to other ports.

Bandwidth

Bandwidth is the range of frequencies within which the performance of the antenna, with respect to some characteristic, conforms to a specified standard [21]. In this design task, the figure of merit to evaluate in the specific frequency band are the reflection coefficient and the probability of detection (see the section Theories and Techniques of OTA for its definition).

2.3.2 Log-periodic dipole array

Log-periodic dipole array (LPDA), invented by Dwight Isbell and Raymond DuHamel, is a directional antenna, composed of multiple elements (usually dipoles), for wideband applications. LPDA consists of several dipole elements whose size and spacing between each other increases geometrically with a factor k from the smallest element to the largest element. The purpose of the log-period configuration is to achieve the broadband properties. The characteristics e.g. relatively uniform input impedances, reflection coefficients, and radiation patterns of LPDA is frequency independent over the desired frequency band. The reason for this is that the size and spacing of the dipoles are varying gradually and each dipole is responsible for a sub-frequency band centered at a particular frequency point determined by the size of the dipole. In each sub-frequency band, the characteristics of the antenna are similar to each other. If the scaling factor k is selected properly, e.g. the whole desired frequency band is fully covered by all the sub-frequency band, the performance of the LPDA is roughly the same in the whole frequency band.

An LPDA can be fed simply a with balanced feeder and the alternating element connections enable all the adjacent elements be fed with 180^o phase shift.

If the LPDA is designed to operate on the frequency range between f_1 and f_n, where f_1 is the lowest frequency and f_n is the highest frequency, the number of the antenna element n and the scaling factor k can be carefully selected so that the electrical characteristics will almost keep constant within the frequency range. Other geometrical parameters such as the length of each dipole and the distance between dipoles will also have influence on the electrical characteristics of the LPDA.

The frequency, length of each dipole and separation between each other are defined by the following equations:

$$f_i = \frac{f_n}{k^{n-i}} \tag{2.35}$$

$$l_i = l_n \times k^{n-i} \tag{2.36}$$

$$d_{i,i-1} = d_{n,n-1} \times k^{n-i} \tag{2.37}$$

where i is the index of the antenna element ($i = 1,2,...,n$) Typically, the scaling factor k is slightly larger than 1, but its value cannot be too high.

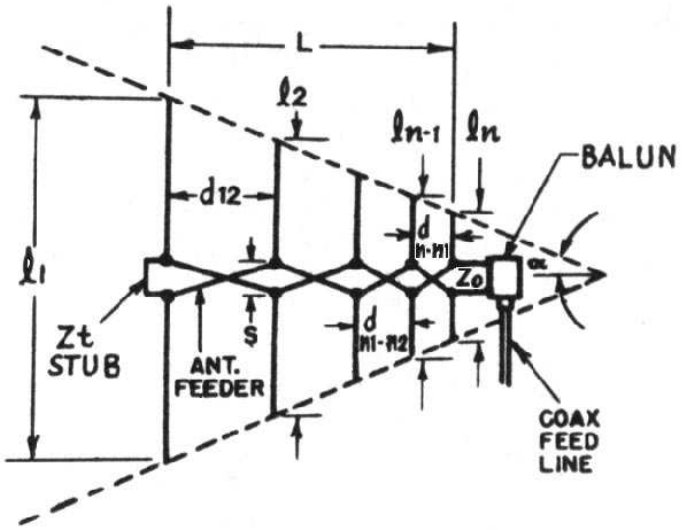

Figure 2.3: Illustration of a log-period dipole array

2.3.3 Eleven antennas

The Eleven antenna is a specific kind of LPDA, invented by Per-Simon Kildal at Chalmers University of Technology in 2006 [3]. It is referred to as the Eleven antenna because a pair of parallel half-wave dipoles is in the configuration of 11. The number of dipole pairs is determined according to the specific operation bandwidth. In general, the wider is the frequency band that the antenna is supposed to operate in, the more the number of dipoles is needed. What makes the Eleven antenna differ from the LPDA is that the phase center in an LPDA varies with frequency, whereas in the Eleven antenna it is locked to the ground plane in spite of the change of frequency.

Then, the geometry of the Eleven antenna was evolved to the so-called circular Eleven antenna [22–26]. The analysis of the antenna can be found in [5–7, 27–30]. Recently, the Eleven antenna has been evolved further to the so-called truly conical Eleven antenna for high frequency applications [31].

The Eleven antenna has a wideband performance. It can have up to 8 ports for dual polarization. Therefore, it is very suitable for MIMO applications.

2.3.4 Research activities on other UWB antennas at Chalmers

In addition to the Eleven antenna, Antenna Division at Chalmers has been developing other wideband antennas. The hat-fed reflector antenna is a kind of wideband antenna [32–38] that can be applied in satellite communication systems. The self-grounded Bowtie antenna [39–44] is another kind of ultra-wideband antenna, and it can be applied under many scenarios, for instance, UWB radar and medical detection. The quad-ridge flare horn is an ultra-wideband antenna [45] applied mainly in radio telescopes. But all

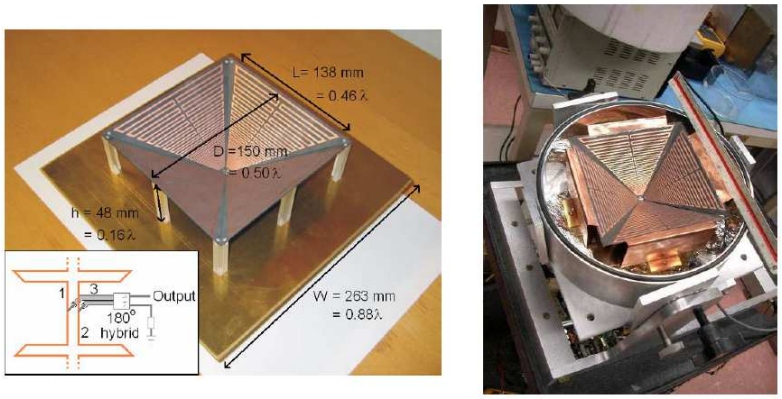

Figure 2.4: Photograph of the manufactured 1 to 13 GHz lab model eleven antenna in [30]

of these antennas are non-planar. So the planar Eleven antenna is chosen as the theme in this thesis project.

2.4 Genetic Algorithm for Antenna Design

Genetic algorithm (GA) is an adaptive heuristic search algorithm, introduced by John Henry Holland, which mimics the nature evolution process following the principles of 'survival of the fittest' laid down by Charles Darwin. GA is a powerful tool widely used in the optimization problems. Applying this algorithm will result in the survival of the samples with the best performance with respect to certain characteristics on which the algorithm take effect. The mechanisms of how genetic algorithm works in the antenna design and the professional terms are described in the following part.

2.4.1 Genes and Chromosomes

In the design of a particular antenna, usually there are many parameters that will influence the shape of the antenna. The designer can change the parameters in the range that ensures the shape and size of the antenna is acceptable so that the specific goal, e.g. directivity, reflection coefficients, radiation pattern, etc. can be fulfilled. These parameters are called genes since they will be carried to the next generation in a way that mimics the behaviour of reproduction if the performance of the sample with these genes is acceptable. A chromosome is a set of genes as a whole that fully determines the shape and performance of an antenna.

2.4.2 Number of population

To do the optimization with genetic algorithm, usually large numbers of antenna samples with different genes will be generated. Quite often the value of the genes are normally distributed in a specific range that satisfies the design requirement on the size of the

antenna. The total number of the antenna samples simulated is the number of population in one generation. Obviously the larger the number of population, the better results it will give. But the drawback is computation time and cost will also increase. So it's very important to choose the proper number of population.

2.4.3 Fitness function, Elites and Civilians

For the antenna optimization, there is always at least one goal. To measure how close the generated antenna samples are to achieving this goal, a fitness function is defined as a figure of merit. It is a function designed by the antenna design according to his or her wish as long as it can represent the performance of the aspect being optimized. The fitness function will give a value, which represents the performance, for each antenna sample. Usually the higher the value it gives, the better the performance is. A specific value is defined as the threshold. Samples with the fitness values higher than the threshold are classified as elites and the rest are civilians.

2.4.4 Roulette Wheel selection

It is necessary to keep the civilians although they do not show good performance in the first generation. If all of these samples are discarded in this stage, their unique genes that may result in the improvement of the performance will be lost forever and therefor it is impossible to get the best obtainable result. To select the eligible civilians and give them the chance to produce children, several strategies, e.g. Boltzmann selection, Tournament selection, Steady state selection, Truncation selection, etc. can be employed. Roulette Wheel selection is a quite popular method in all the selection techniques and it is used in this antenna design task. It select the civilians by chance according to their fitness values. The higher the fitness value is, the more likely the sample will be selected. The summation of the fitness value of every civilian is considered as a whole wheel and each civilian's share on the wheel is corresponding to the percentage of its fitness value in the whole fitness value. If the wheel is rotated and it will stop after a while. The stick will randomly point to one civilian and that one is thus picked out and given the chance for reproduction. The possibility that one individual civilian is

$$p_i = \frac{f_i}{\sum_{j=1}^{M} f_j} \tag{2.38}$$

where M is the number of civilians and f_i is the fitness value of the ith civilian. It is also called fitness proportionate selection since the chance one civilian will be selected is proportional to its fitness value. Figure 2.5 is just for the purpose of illustration so that the reader will understand easily how Roulette Wheel selection works. In the real application, the number of civilians are far more than 8.

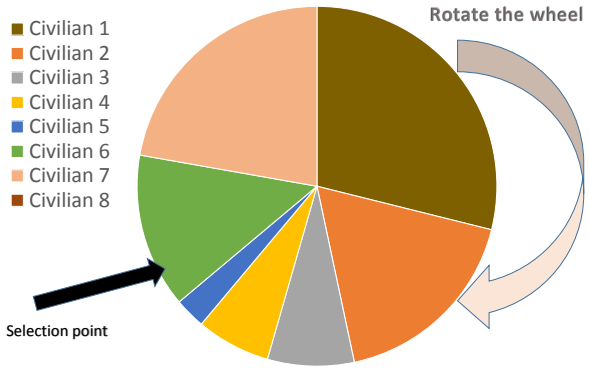

Figure 2.5: Illustration of the Roulette Wheel selection

2.4.5 Crossover

The genes of all the elites and the eligible civilians obtained from the Roulette wheel selection in the first generation will be passed on to the next generation by means of crossover. It is a process, analogous to biological crossover, which produces children solutions from more than one parent solutions. The performance of the individuals, no matter the elites or the civilians, is not good enough, since not all the genes in the chromosome are good. It's very likely that some genes are bad, even in the elites, and thus the performance is deteriorated. The reason for doing crossover is to improve the performance by mixing the genes of parents so that good genes are preserved and the bad ones are dropped. There are many crossover techniques. Here several of them that are most widely used are reviewed generally.

One-point crossover

A single point on the chromosomes of the parents is randomly selected. The genes beyond that point in either chromosome are swept between the two parents.

Two-point crossover

It's similar to the one-point crossover except that there are two crossover points, also randomly selected, on both chromosomes of the parents. The genes between the two points are swapped between the two parents.

Uniform crossover

Both one-point crossover and two-point crossover focus on the mix of chromosomes in terms of string of genes. Uniform crossover is a sort of generalized method of them. Uniform crossover focuses on the mix of chromosome on the individual level of genes rather than the segment level. In the uniform crossover, every gene in the chromosomes of both parents are compared and are swapped with a fixed probability.

2.4.6 Mutation

Mutation is a genetic operator, analogous to biological mutation, which modifies one or more genes from the original value so that the genetic diversity is maintained and the solution is prevented from premature convergence. Usually the probability of mutation is set very low (typically less than 5%). In this antenna design project, mutation is neglected since usually it will do more harm than good and the time is limited.

2.4.7 Next generation

Most often the performance of the elites in the next generation will be better than, at least not worst than, that of the elites in the previously generation if the number of population is large enough. If the result converges, i.e. the difference of the best individuals between generations is negligible, or the goal of the design is achieved, the optimization can be terminated.

2.5 Basic Theories of Wireless Communications

2.5.1 AWGN channel

The additive white Gaussian noise (AWGN) channel model is a channel whose sole effect is addition of a white Gaussian noise process to the transmitted signal . The channel can be described mathematically by the relation

$$r(t) = s(t) + n(t) \tag{2.39}$$

where $s(t)$ is the transmitted signal, $n(t)$ is the zero-mean white Gaussian noise and $r(t)$ is the received signal.

2.5.2 Rayleigh Fading

AWGN is a simple channel model useful in analyzing the satellite and deep space communication links in which the signal propagates following the line-of-sight path between the transmitter and the receiver. In many wireless applications, however, there might be no direct line-of-sight path between them. For instance, the direct path between the mobile users and the base station is usually blocked by buildings. In this case, multiple paths may exist between the user and the base station resulting from reflection, scattering and diffraction.

The overall signal at the receiver side is a summation of the signals in these different paths. The signals will add constructively or destructively according to their phases due to different length of the paths. Besides, when the distance between the transmitter and the receiver changes over time, e.g. the mobile user is moving, it may also cause the variation of the received signal. This effect is called fading, and it's a widely existed phenomenon in the wireless communication.

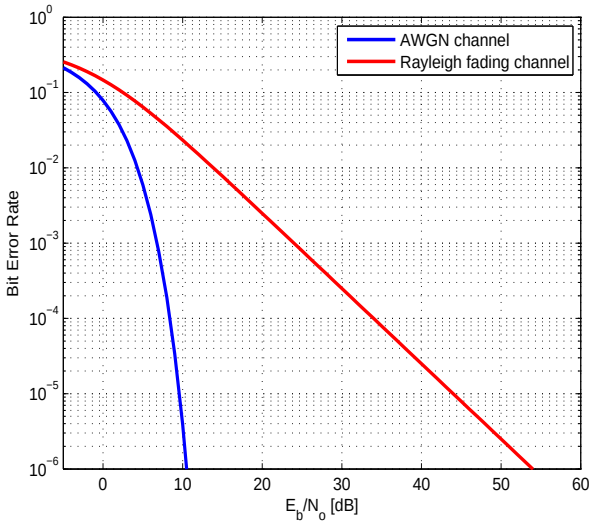

Figure 2.6: Theoretical bit error rate for BPSK as a function of E_b/N_0 over AWGN and Rayleigh fading Channels

In the analysis of radio signals transmitted or received by wireless devices like mobile phone, the statistic model of Rayleigh fading is usually assumed for the communication channel. It applies on the situation where there is no dominant line-of-sight component between the transmitter and the receiver.

In order to show the difference between the AWGN channel and the Rayleigh fading channel with respect to the performance of bit error rate (BER), binary phase-shift keying (BPSK) is assumed here as the modulation format since it's the simplest case. For other more complicated modulation formats, the degradation on BER due to fading is similar to the BPSK case.

For AWGN channel, the BER is

$$P_{b,AWGN} = \frac{1}{2} erfc(\sqrt{\frac{E_b}{N_o}}) \tag{2.40}$$

For Rayleigh fading channel, however, the BER is

$$P_{b,Rayleigh} = \frac{1}{2}(1 - \sqrt{\frac{\frac{E_b}{N_o}}{1 + \frac{E_b}{N_o}}}) \tag{2.41}$$

It can be seen from figure (2.6) that the difference of the needed $\frac{E_b}{N_o}$ to reach a low BER (usually 10^{-5} is the level assumed for a reliable communication link) between the AWGN case and Rayleigh fading case is very huge. It's unrealistic to provide very high symbol energy or bit energy for the system with a Rayleigh fading channel to make it work. One way to solve this problem is to employ the MIMO diversity so that the fading due to multipath propagation is mitigated.

2.5.3 MIMO diversity and maximum ratio combining

Multiple-input and multiple-output (MIMO) is a technology in modern wireless communication that multiple transmit and receive antennas are used and the signals at the transmitter side and the receiver side are combined in such a way that the BER will be improved compared with the case where only a single antenna is used in each side.

Diversity combining of signals in independent fading paths will mitigate the fading effect since the probability is very low for all the signals to suffer from deep fading, under which condition the BER is very bad, simultaneously.

Linear combination techniques are widely applied to achieve diversity. The signal at the output of the combiner in the receiver side is a sum of signals from individual fading paths with different weight. The same signal $S(t)$ is send through M different transmit antennas with weight r_i and phase θ_i through the i_{th} antenna. At the receiver side, the phase for each branch will be removed by multiplying a factor with the phase $-\theta_i$ and a coefficient α_i determining the weight. This process is called co-phasing, which requires the phase information at the transmitter to be known. Then, all of the signals from M different diversity branches are added together to form the signal at the linear combiner output (see figure 2.8).

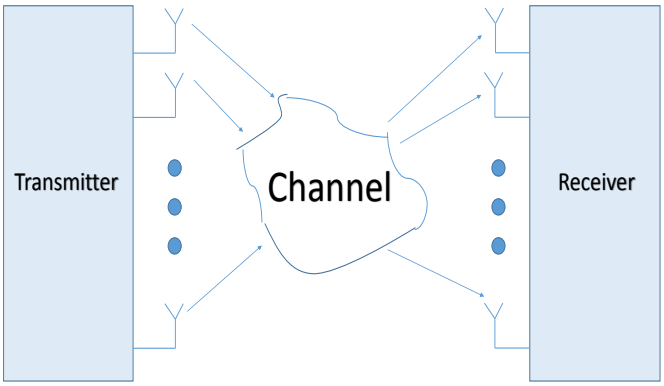

Figure 2.7: Diagram of a MIMO system

$$\alpha_i = a_i e^{-j\theta_i} \tag{2.42}$$

$$\beta_i = b_i e^{j\theta_i} \tag{2.43}$$

The SNR for the ith branch is

$$\gamma_i = \frac{|\alpha_i \beta_i|^2 E_b}{|\alpha_i|^2 N_i} \tag{2.44}$$

where E_b is the energy per bit in the signal S(t) and N_i is the power of the white Gaussian noise $n_i(t)$ in the ith branch.

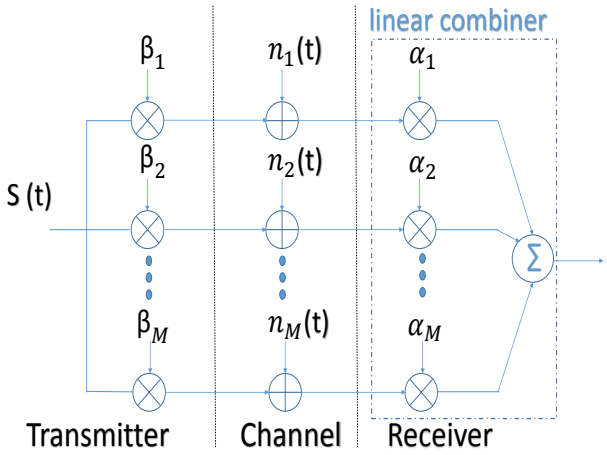

Figure 2.8: Illustration of diversity in system block

The total SNR at the output of the combiner is therefor

$$\gamma_{\sum} = \frac{\sum_{i=1}^{M} |\alpha_i \beta_i|^2 E_b}{\sum_{i=1}^{M} |\alpha_i|^2 N_i} \tag{2.45}$$

When only one transmitting antenna is used (one bitstream scenario), equivalent to single-in and multiple-out (SIMO) case, the scheme of maximal-ratio combining (MRC) is applied, in which the weight a_i of the ith branch is selected as optimal value that maximizes the total SNR.

$$a_i = \frac{\beta_i}{N_i} \tag{2.46}$$

The corresponding SNR is the sum of the SNR of all the M diversity branches

$$\gamma_{\sum} = \sum_{i=1}^{M} \gamma_i \tag{2.47}$$

2.5.4 Zero forcing

For the case that the transmitter is with full spatial multiplexing (two-bitstream scenario), the zero-forcing (ZF) filter in the receiver separating the the received signal into the transmitted streams is defined by [46]

$$\mathbf{G}_{ZF} = \sqrt{\frac{M_T}{E_s}} \mathbf{H}^{\dagger} \tag{2.48}$$

where M_T is the number of transmitting antenna, $\mathbf{H}$ is the channel matrix and E_S is the symbol energy.

The power (equal to the SNR due to the unit noise assumption) of the ith stream becomes [47]

$$P_i = \frac{1}{[(\mathbf{H}^H\mathbf{H})^{-1}]_{i,i}} \tag{2.49}$$

where the superscript H denotes conjugate transpose and $[\mathbf{X}]_{i,i}$ represents the ith diagonal entry of the matrix $\mathbf{X}$.

2.6 Theories and Techniques of OTA

This section reviews the theories and technologies involved in Over-the-Air (OTA) tests. Most of the content here is collected from relevant parts of [19, 48–50].

2.6.1 RIMP

Multipath is such a kind of environment consisting of several independent incoming waves, whose amplitudes, phases, polarizations and the angles of arrival (AoA) are uncorrected to each other, at the receiving side [19]. The rich isotropic multipath environment is the hypothetical multipath environment defined as a reference, for the convenience of measurement, that assumes uniform distribution of AoA of the incoming waves within 4π steradian and polarization balance, where the term 'rich' means the number of incoming waves is large, typically more than 100 [48].

2.6.2 RLOS

Line-of-Sight (LOS) propagation of an electromagnetic wave means the direct ray from the transmitter to the receiver is unobstructed, i.e., the transmission path is not established by or dependent upon reflection or diffraction. But antenna devices in modern communication systems are not limited to this simple type. Especially for the case of the micro-base station which is located in the multipath environment together with the user and the wireless device, the user and the micro-base station may even be located in the same room. In this situation, there may be a significant LOS contribution to the wireless channel between them. The LOS contribution will in a mobil wireless system be random due to the arbitrary orientation and location of the user, and is therefore herein referred to as a random-LOS [50]. The RLOS is a scenario, taking into account the user statistics.

Antennas often do not have a directive beam, but rather have several arbitrarily oriented beams. Besides, the orientation of a wireless device, e.g. cell phone, is a kind of randomness. Then, when the distance between the base station and the user is short (the case for micro base station) or when the operating frequency is high at millimeter waves, the scenario of random line-of-sight may dominate.

2.6.3 OTA tests and a real-life hypothesis

OTA tests are widely applied and becoming increasingly important nowadays since it allows device manufacturers and network operators to predict the performance like the reliability, safety and performance capabilities, etc. of real-world wireless devices in modern communication.

To emulate the real-life environment, a new systematic characterization approach is proposed in [48] for OTA measurement evaluation of wireless devices in RIMP and RLOS. The RLOS environment and the RIMP environment are two different limiting environments (or margin environments) that are not like to exist in reality. The real-life environment is somewhere in between, e.g. neither necessarily fulfilling the requirement of 'rich' (number of incoming waves is not enough to be classified as rich) nor can be treated as pure-LOS as the multipath exists. Still, it's of great value to study the performance of the device under these two environments as it gives a reference to predict the real-life case.

A real-life OTA hypothesis which states that *if a wireless device works well in both RIMP and random-LOS, it will also work well in real-life environment* is proposed in [48]. The RLOS and RIMP environments are linked to real-life environments by the hypothesis and a new method to optimize the wireless network taking into account the user statistics is proposed in [49]. The RLOS environment can be analyzed with the ViRM-lab, a computer program investigating performance of wireless terminals in multipath with many arbitrary incident waves [51] based on standard receive antenna equivalent circuits [52]. The way of characterizing the micro-BTS in terms of PoD in both RIMP and RLOS is proposed in [50].

PoD

The bit error rate (BER) is the percentage of bits that have errors relative to the total number of bits received in the receiver. BER is widely used as a criterion in wireless communication to measure the performance of the communication system. In advanced wireless systems, the bits are gathered in groups so that the bit group is less sensitive to errors than the single bit is. For this reason, the group error rate (GER) is introduced and an ideal error correction receiver is defined in [53], when a dynamic channel with time-varying fading is considered, as

$$\mathrm{GER}_{\mathtt{av}}(P_{\mathtt{av}}) = \mathrm{CDF}(P_{\mathtt{t}}/P_{\mathtt{av}}) \tag{2.50}$$

where P_{av} is the average of received power and $P_{\mathtt{t}}$ is the threshold power level, under which the digital receiver with the error correction codes does not function correctly but above which it functions. The average throughput date rate T_{PUT} is defined in [50] as

$$T_{\mathtt{PUT}}(P_{\mathtt{av}}) = T_{\mathtt{PUT,max}} \times [1 - \mathrm{CDF}(P_{\mathtt{t}}/P_{\mathtt{av}})] \tag{2.51}$$

where $T_{\mathtt{PUT,max}}$ is the maximum achievable throughput for the system and CDF is the cumulative distribution function of the channel power. The PoD as a function of the average received power is defined as

$$\begin{aligned} \mathrm{PoD}(P_{\mathtt{av}}) &= T_{\mathtt{PUT}}(P_{\mathtt{av}})/T_{\mathtt{PUT,max}} \\ &= 1 - \mathrm{CDF}(P_{\mathtt{t}}/P_{\mathtt{av}}) \end{aligned} \tag{2.52}$$

Bitstream is defined as the independent information-carrying modulated wave vectors coming in on each (or some) of the ports of the transmitting antenna [50]. The PoD for a single bitstream case using Maximum-Ratio Combining (MRC), in which the output is a weighted sum of all branches [54] and for two bitstreams case using a simple Zero Forcing (ZF) algorithm[47] is of interest in this paper.

3

Design and Optimization

This chapter first describes the layout and the geometrical dimensions of the antenna designed. Then the purpose for the design of the antenna and the application environment is explained. The modeling procedure and detailed geometrical design are elaborated afterwards. The criterion to evaluate the antenna and conditions under which the antenna will be examined are discussed thereafter. The reason for employing the cst-matlab combined modeling approach is justified and the detailed procedure of modeling and optimization scheme is elaborated in the end.

3.1 Layout

The antenna consists of two branches located in different horizontal planes separated by 3 mm vertically. For each branch there are two identical groups of dipoles with the dipole elements cascaded within the group. A transmission line connects the innermost dipole of the two groups. A pair of coaxial cable with characteristic impedance of 50 $Ohms$ are connected to the middle of the transmission line and excite the antenna with differential modes.

In this design, each branch contains eight pair of dipoles. The sizes of the eight dipole pairs are in geometric progression with a scaling factor k between the previous pair and the next pair. The dipole pairs are made of copper lying on substrate board made of $RogersRO4003C$. Part of the substrate board of the high branch is cut so that the radiation field of the low branch is not obstructed. The copper ground plane reflects the backwards radiation and therefore the energy efficiency is improved.

The supporting structure between the substrate of the high branch and the low branch, the low branch and the ground plane are made with Teflon since its existence will not influence the radiation field or the reflection parameter. The total size of the antenna is $337(sidelength) \times 337 \times 37(hight)\text{mm}^3$ (see Fig. 3.1 and details in Fig. 3.2).

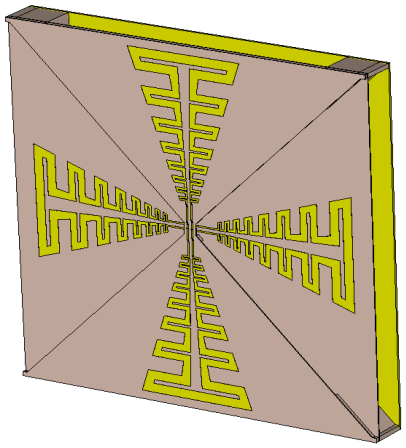

Figure 3.1: CST model of the present flat MIMO Eleven antenna with a size of 337×337×37 mm^3.

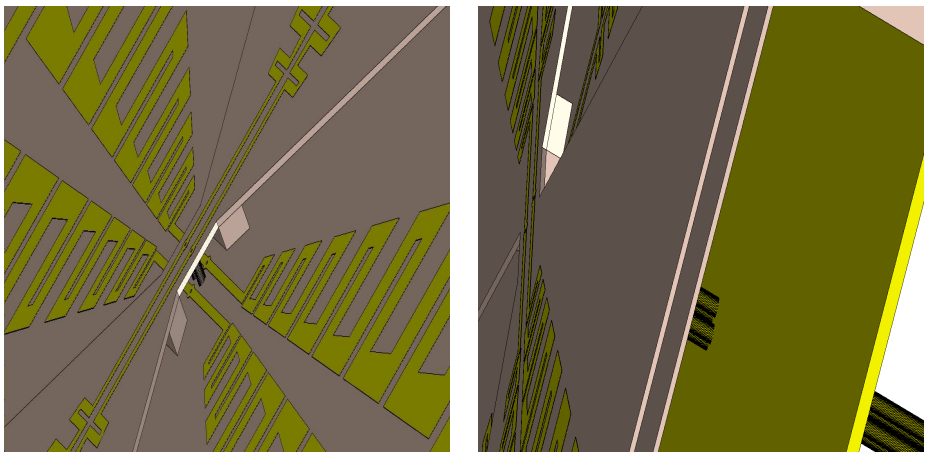

(a) Transmission line part (b) Side view

Figure 3.2: Detail of the CST model of the flat MIMO Eleven antenna.

3.2 Application of the Antenna

The antenna is designed to serve as a micro-base antenna for 5G communication. It will find wide application in small area, especially in a house, focusing on high data rate transmission. The antenna can be installed on the ceiling and function as a hotspot. When a group of people are having a meeting together, it can link these people by wireless network and therefor data is allowed to be shared among them simultaneously at a high speed. If the hight (H) of the ceiling is $3m$, the area (A) covered by the antenna is around 60 m^2 (see Fig 3.3).

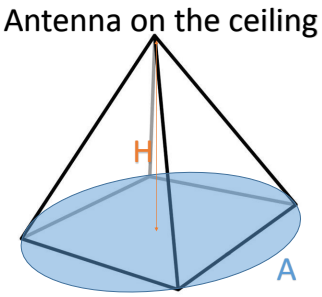

Figure 3.3: Illustration of the application of the antenna

3.3 Modeling Procedure

The antenna is to be designed to be dual polarized and therefore the it is composed of two branches orthogonal to each other, i.e. the high branch and the low branch, responsible for orthogonally polarized waves. The prototype of the antenna originates from an antenna designed in Chalmers University of Technology in the year 2006 [3]. The main differences between the old one and the antenna designed in this thesis project are that the antenna proposed in [3] is used as a feed in the reflector antenna and is of non-planar type while the antenna designed here is used as a whole antenna for micro-base station and is of planar type so that the manufacture cost is cut down.

The antenna is supposed to work over the frequency band of 1.6 GHz to 2.8 GHz, a relative bandwidth of more than 50%. In order for the criterion of wide bandwidth to be satisfied, several techniques can be applied. In this design, the method of cascading dipoles pairs is employed.

3.3.1 Description of the basic configuration

For each dipole, the geometrical variables are the length of the dipole (l), gap width of the dipole (d_c), width of the dipole (d_a), arm width of the dipole (w_a), transmission line width (w_t), separation between the transmission line (S). The distance between two dipoles in a pair (d), the separation between transmission lines (S) and the width of the each transmission line (w_t) are also optimizable geometrical parameters (see figure 3.4 and figure 3.5).

These geometrical parameters are expressed as the following:

$$f_{\mathtt{geo,i}} = \frac{f_{\mathtt{geo,max}}}{k^{\mathtt{i-1}}} \tag{3.1}$$

$$\lambda_{\mathtt{geo,i}} = \frac{c}{f_{\mathtt{geo,i}}} \tag{3.2}$$

$$d_{\mathtt{i}} = k_d \times \lambda_{\mathtt{geo,i}} \tag{3.3}$$

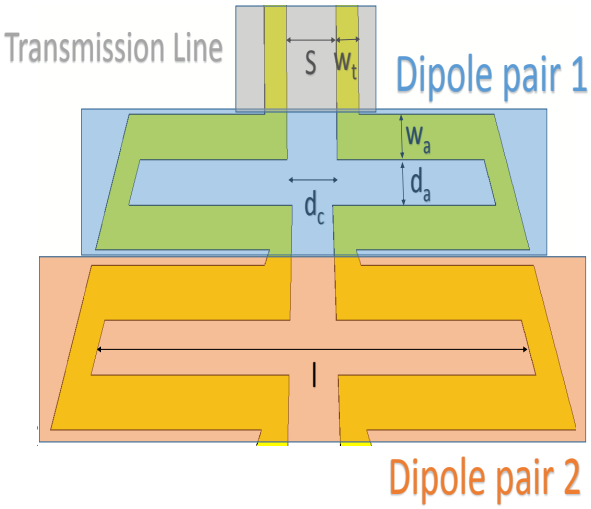

Figure 3.4: Illustration of the geometrical parameters

$$d_{\mathtt{a,i}} = k_{d_a} \times \lambda_{\mathtt{geo,i}} \tag{3.4}$$

$$d_{\mathtt{c,i}} = k_{dca} \times \lambda_{\mathtt{geo,i}} \tag{3.5}$$

$$w_{\mathtt{a,i}} = k_{w_a} \times \lambda_{\mathtt{geo,i}} \tag{3.6}$$

$$l_{\mathtt{i}} = k_l \times \lambda_{\mathtt{geo,i}} \tag{3.7}$$

where i stands for the ith dipole.

So, the genes in the genetic algorithm for optimization are $f_{\mathtt{geo,max}}$, k, k_d, k_{da}, k_{dc}, k_{wc}, k_l, S and w_t.

Coordinates for making the antenna:

$$\alpha = arctan(\frac{dc/2}{d/2}) = arctan(\frac{k_{dc}}{k_d}) \tag{3.8}$$

$$\beta = atan(\frac{l+2w}{d}) \tag{3.9}$$

$$\begin{cases} x_A = \dfrac{d_c - d_a}{2} - w & \text{(3.10a)} \\ y_A = \dfrac{l}{2} + w - tan(\beta)(\dfrac{da}{2} + w) & \text{(3.10b)} \end{cases}$$

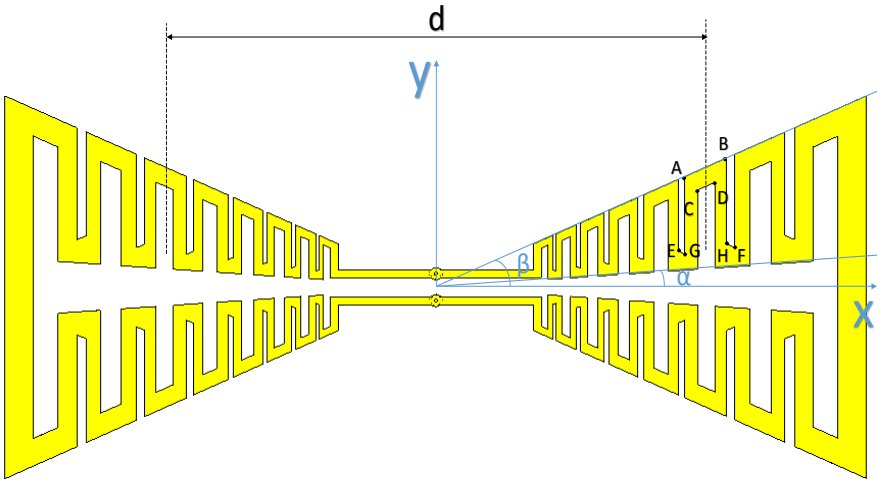

Figure 3.5: Design drawing of the antenna

$$\begin{cases} x_B = \dfrac{d_a + d_c}{2} + w & (3.11a) \\ y_B = \dfrac{l}{2} + w + tan(\beta)(\dfrac{da}{2} + w) & (3.11b) \end{cases}$$

$$\begin{cases} x_C = \dfrac{d_c - d_a}{2} & (3.12a) \\ y_C = \dfrac{d_c - tan(\beta)da}{2} & (3.12b) \end{cases}$$

$$\begin{cases} x_D = \dfrac{d_a + d_c}{2} & (3.13a) \\ y_D = \dfrac{d_c + tan(\beta)da}{2} & (3.13b) \end{cases}$$

$$\begin{cases} x_E = \dfrac{d_c - d_a}{2} - w & (3.14a) \\ y_E = tan(\alpha)x_E + w & (3.14b) \end{cases}$$

$$\begin{cases} x_F = \dfrac{d_a + d_c}{2} + w & (3.15a) \\ y_F = tan(\alpha)x_F + w & (3.15b) \end{cases}$$

$$\begin{cases} x_G = \dfrac{d_c - d_a}{2} & \text{(3.16a)} \\ y_G = \dfrac{d_c - tan(\alpha) d_a}{2} & \text{(3.16b)} \end{cases}$$

$$\begin{cases} x_H = \dfrac{d_a + d_c}{2} & \text{(3.17a)} \\ y_H = \dfrac{d_c + tan(\alpha) d_a}{2} & \text{(3.17b)} \end{cases}$$

3.3.2 *PoD*

To minimize the P_{av}/P_t under a certain PoD is a design criterion to reach in this thesis work. In decibel unit, P_{av}/P_t is $P_{av}[dB] - P_t[dB]$, which means how many dB the averaged receiving power (P_{av}) over the threshold power (P_t) is required so that the desired PoD can be achieved. The less the power is required, the higher the power efficiency is reached. Here 95% of the PoD level is selected to evaluate the P_{av}/P_t value since this PoD level is good enough for the application of the antenna here.

For the RIMP case, the PoD is of interest over the whole area whereas for the RLOS cases, the PoD is calculated within a certain solid angle area from the transmitting antenna (such as the antenna of a base station), illustrated as a red window on a sphere in Fig. 3.6. It is the intersection between the sphere and a right pyramid with an 4-sided base whose apex is on the center of the sphere. In this work, The angle between the two pairs of the side faces facing each other in the pyramid is chosen as 120°.

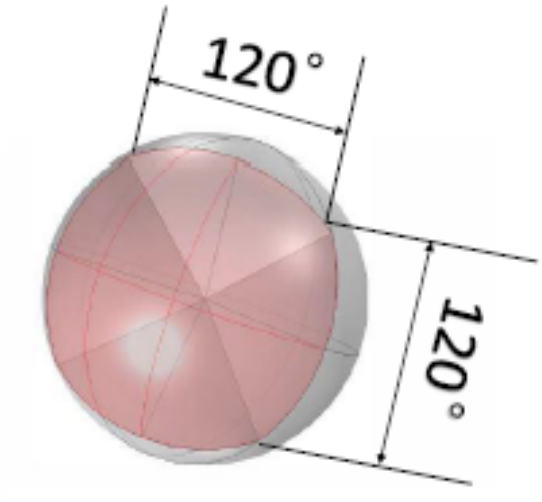

Figure 3.6: Illustration of the solid angle area for PoD calculation in RLOS cases

3.3.3 S_{11}

S_{11} is usually a important criterion to take into account when it comes to the design of an antenna. It describes the percentage of the energy reflected to the voltage or current source relative to the the energy used to excite the antenna at in input port. The lower the value of S_{11} is, the higher the energy efficiency it achieves. For a practical antenna, the S_{11} is usually around -10 dB.

In this design, each branch of the antenna consists of four parts, i.e., the excitation port, the coaxial cable, the transmission line and the antenna. Reflection exists on the interface of the excitation port and the coaxial cable, the coaxial cable and the transmission line, the transmission line and the antenna. To quantify the the total energy reflected, the total S_{11} -the reflection between the port and the coaxial cable- is of interest (See figure 2.1).

3.3.4 Parameter sweeping

It is observed that in this design that both the S_{11} and the PoD are influenced by the shape of each dipole pair in the antenna. The number of the dipole pairs does not influence the S_{11} but it is of great importance to the PoD over frequencies. If the number of the dipole pairs are not enough, in some frequencies-usually around the highest or the lowest frequency-the P_{av}/P_t needed to reach the PoD requirement is extremely high. It means that there is a low limit on the number of dipole pairs in order for the antenna to cover the frequency band. It is observed that the minimum number of dipole pairs required in this design is eight. It's possible to cascade more dipole pairs, but it will enlarge the total size of antenna and therefore the manufacture cost is raised up.

The adjustable geometrical parameters are the highest geometrical frequency which determines the size of the smallest dipole pair, width of the dipole arm, total width of one dipole, horizontal space in one dipole, vertical space in a dipole pair, scaling factor between each dipole pair, width of the transmission line, separation between transmission lines.

The aim of parameter sweeping is to decide the possible range for the optimization in the next stage. The approach to tune the parameters are in two steps. First, tune only one parameter at a time and keep other parameters unchanged. The purpose for this is to figure out the influence of each parameter on the S_{11} and PoD and find the rough range of each parameter in which the S_{11} and PoD are acceptable. Many parameters indeed play a big role on the performance, the influence of others, e.g. d_a,d_c, seems negligible. Then group the parameters together and sweep them simultaneously to study the total effect of them on S_{11} and PoD to get the refined range of the parameters so that the time needed for the optimization is reduced. It's worth to mention that another important aspect of parameter sweeping is that it gives intuitive understanding of how the shape of the antenna influence the performance.

3.3.5 Matlab-CST combined modeling scheme

Usually it's very convenient to build up the antenna model in CST Microwave studio if the structure is not too complicated. In this design, however, it is quite difficult to do the parameter sweep or the optimization if the model is built only in CST. Although the antenna structure seems not so complicated at first glance, the whole structure is at the risk of collapse when the some parameters changed. For instance, when the separation of the transmission line is reduced and the length of the arm of dipole pair one is fixed, the transmission line will be disconnected from the dipole antenna (see Fig 3.4). The size of the substrate board is determined by the larger one in the high and low antenna branches. an *'if'* statement is therefore needed to pick up the right size for the board. The number of dipole pairs needed to cascade is also unknown before simulation. It's cumbersome to tune it and simulated the structure in CST one at a time. Matlab simplifies the tedious task by allowing it to be set as a variable in code and a for loop can be used to control the duplication of the dipole pairs. The antenna is composed of many parts, e.g. the high branch and the low branch, the dipole pairs, the transmission line, the substrate board, the supporting structure between the board and ground plane etc. Thus it has the nature of fallibility when it comes to the building of the model and tuning of the parameters. Programming in matlab provides the freedom to build and test the structure part by part so that it's easier to find the errors and fix them.

Due to the facts mentioned above, it's necessary to employ the matlab-CST combined modeling scheme in which flow control and loops are realizable so that more flexibility and freedom on control is enjoyed. The detailed procedure is described as follows.

After the model is built is CST, it will generate a .mod file in which every step to build the model is documented as visual basic language. A matlab script can be written to read the information in the `.mod` file and generate a corresponding `.m` file in which control flows and loops can be added and geometrical parameters defining the shape of the antenna are treated as variables. In this stage, programming method is employed to control the way to build the model according to the specific requirements of the design by the antenna designer.

The geometrical parameters are generated as random variables uniformly distributed in the range obtained from the parameter sweeping previously. Large numbers of antenna samples with the random geometrical parameters are therefore produced. The number of samples generated can be controlled manually by setting it as parameter in the matlab code. Since the geometrical parameters are generated randomly, it is possible that for some combinations of the parameters the structure collapses due to e.g. the disconnection between the dipole pairs and transmission line or between the coaxial cable and the transmission lines. Sometimes although the structure does not collapse, the manufacture cost is quite high because the size of the smallest part (often the width (w_a) of the arm or the gap (d_a) of the first dipole pair) of the antenna is very tiny. So it's necessary and convenient to make a matlab script to filter away these samples.

Finally, a bunch of `.mod` files with visual basic language documenting the structure of the antenna is produced by the matlab script as antenna samples. Then these samples are simulated in CST.

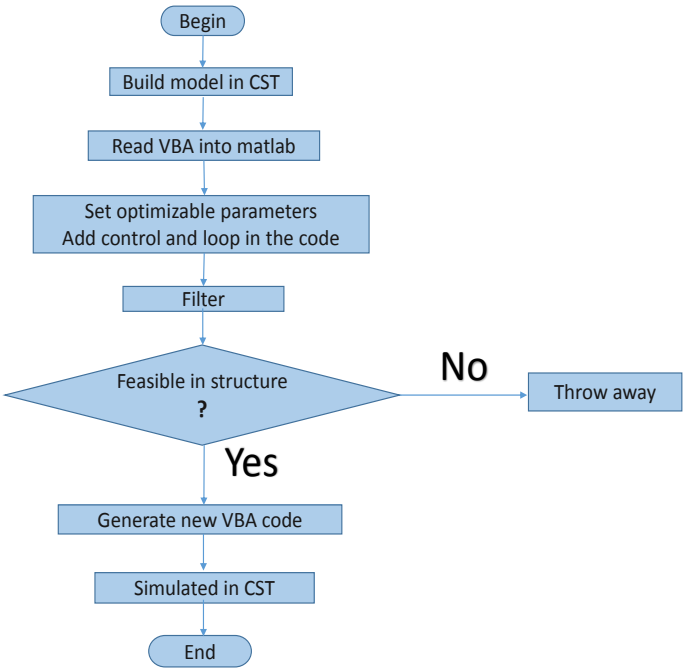

Figure 3.7: Flowchart of the matlab-CST combined modeling scheme

3.4 Optimization Scheme

Genetic algorithm is employed in this design in the optimization process. The first generation is generated with geometrical parameters uniformly distributed within specific ranges. Figure 3.7 illustrates the detailed process. In this design, N =400 samples are generated and simulated in one generation.

3.4.1 Fitness evaluation and selection criterion

The total N samples are arranged according to the fitness function. For the application of this antenna the fitness function depends on the highest value of S_{11} over the frequencies of interest, i.e. from 1.6 GHz to 2.8 GHz. For the $i_{\mathtt{th}}$ sample, the highest S_{11} is

$$S_{11,i} = \arg\max_{f} S_{11,i}(f) \tag{3.18}$$

The fitness function of the ith sample is defined as its highest S_{11} divided by the sum of the highest S_{11} of all samples. Here the S_{11} is in decibel. This definition ensures the one with a lower reflection coefficient to be assigned with a higher fitness value since the S_{11} is always negative in decibel.

$$F(i) = \frac{S_{11,i}}{\sum_{i=1}^{N} S_{11,i}} \tag{3.19}$$

The total samples are arranged in descending order of their fitness values, i.e. the higher the fitness value is, the smaller the index in the queue it has. The ones with smallest index value will be selected as elites. Here 15 is set as the number of elites, and the rest of the 400 samples are classified as civilians. So samples with index in the range of 1 to 15 are applicants of elites. Sometimes the one with a index smaller than 15 has a extremely large required $P_{\mathtt{av}}/P_t$ to reach the 95% PoD level and therefor it should be kicked out of the elites group since its performance with respect to PoD is poor.

3.4.2 Two-point crossover

Elites are given the chance to form groups with each one by one and produce children. Each group contains 2 members. A total of ${}^{15}C_2$ groups are formed. Members in the groups, parent 1 and parent 2, produce children by crossover of the chromosomes following the '*two-point crossover*' rule. Each group will produce 2 children. So 210 children will be produced by elites. To keep the number of population unchanged for every generation, 190 children will be produced by civilians. Civilians produce children following the rule of two-point crossover as well, but the way to select the eligible ones and the rule to form group for producing children are different, and the details will be discussed in the next two subsections.

Chromosome of each parent contains 9 genes, corresponding to 9 geometrical parameters. There are two crossover points in the chromosome and therefore it's named as two-point crossover. The crossover points are selected randomly by random variables generated in matlab. Figure 3.8 illustrates how two-point crossover works.

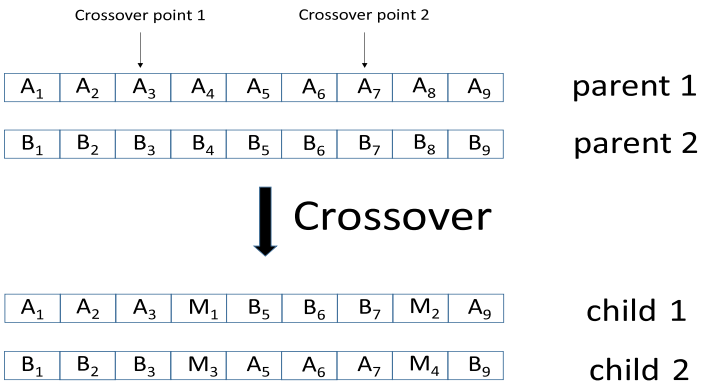

Figure 3.8: Two-point crossover

$$\begin{cases} M_1 = r_1 \times A_{m+1} + (1 - r_1) \times B_{n+1} & (3.20a) \\ M_2 = r_2 \times A_{m+1} + (1 - r_2) \times B_{n+1} & (3.20b) \\ M_3 = r_1 \times B_{m+1} + (1 - r_1) \times A_{n+1} & (3.20c) \\ M_4 = r_2 \times B_{m+1} + (1 - r_2) \times A_{n+1} & (3.20d) \end{cases}$$

r_1 and r_2 are random variables uniformly distributed within 0 to 1. m and n are the index of left and right crossover points, respectively. They are randomly selected in the genes. M_1, M_2, M_3, M_4 are the genes in the chromosomes of children, a mix of genes of parents in the same location on the chromosomes with random percentage r_1 and r_2.

3.4.3 Roulette wheel selection

The eligible civilians are picked following the roulette wheel selection approach. Its principle is already explained in Chapter 2. Here the discussions focus mainly on the mathematical realization to imitate the selection process.

First, arrange the civilians according to their fitness value in ascending order. Define the part of the wheel corresponding to civilian number i as

$$W(i) = \sum_{k=1}^{i} F(i) \tag{3.21}$$

Obviously, $W(i)$ is in the range of 0 to 1. Generate a random variable p uniformly distributed in 0 to 1 as the selection point. When $W(i-1) < p < W(i)$ is satisfied, the civilian number i is selected. This simple algorithm implements the roulette wheel selection in the sense that the probability that an individual will be selected is equal to the share of its fitness value in the sum of the total fitness value of all the civilians. The probability $P(i)$ that civilian number i will be selected is

$$\begin{aligned} P(i) &= P(W(i-1) < p < W(i)) \\ &= W(i) - W(i-1) \\ &= F(i) \end{aligned} \tag{3.22}$$

3.4.4 Civilians crossover

The eligible civilians are selected already. The procedure to perform the crossover for civilians is also two-point crossover, the same as that for elites. What's different is that the number of civilians picked is equal to the number of children they will have. 190 eligible civilians are formed in group of two as number 1 and number 2, number 3 and number 4, ... , number 189 and number 190. Each group will have two children and thus 190 children are produced.

3.4.5 Next generation

For both the elites and the civilians, the feasibility in structure will be checked after crossover. The process of crossover will be repeated until the requirement on the structure is fulfilled, if the antenna samples generated after crossover doesn't have feasible structure. The children of elites and civilians together make up the next generation. The S_{11} and PoD of the new generation are evaluated. If results converge or they are already good enough for the purpose of the application, the process of making the new generation can be terminated.

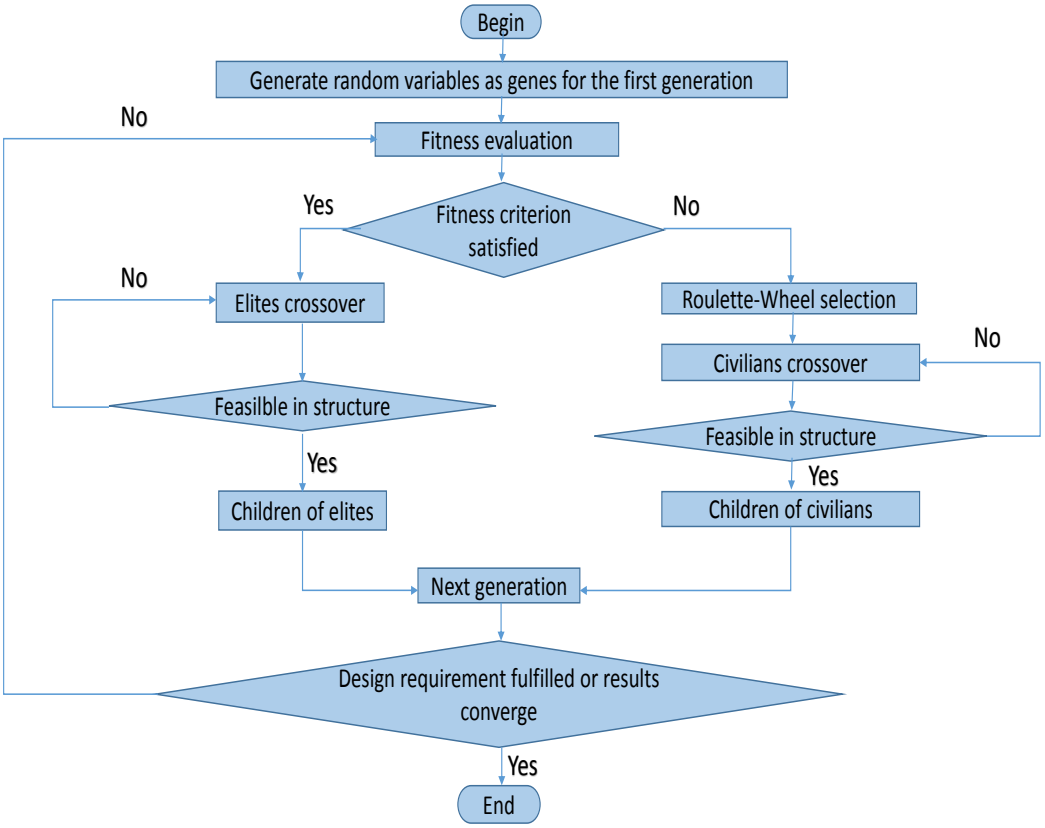

Figure 3.9: Flowchart of the optimization scheme with genetic algorithm

Table 3.1: Final geometrical parameters of the present antenna after optimization

Parameter	Definition ('L' for low branch, 'H' for high branch)	Value
$Lf_{\texttt{geo,max}}$	highest geometry frequency	4.222 GHz
Lk	scaling factor	1.2739
Lk_d	scaling factor of horizontal distance between dipoles pairs	0.7218
Lk_{d_a}	scaling factor of dipole width	0.0097
Lk_{d_c}	scaling factor of gap width in dipole pair	0.0349
Lk_{w_a}	scaling factor of dipole arm width	0.0213
Lk_l	scaling factor of dipole arm length	0.2137
Ls	separation between transmission line	3.1613 mm
Lw_t	width of the transmission line	1.2999 mm
$Hf_{\texttt{geo,max}}$	highest geometry frequency	4.206 GHz
Hk	scaling factor	1.2757
Lk_d	scaling factor of horizontal distance between dipoles pairs	0.7661
Hkd_a	scaling factor of dipole width	0.0093
Hkd_c	scaling factor of gap width in dipole pair	0.0283
Hk_{w_a}	scaling factor of dipole arm width	0.0216
Hk_l	scaling factor of dipole arm length	0.2066
Hs	separation between transmission line	2.9210 mm
Hw_t	width of the transmission line	1.3149 mm

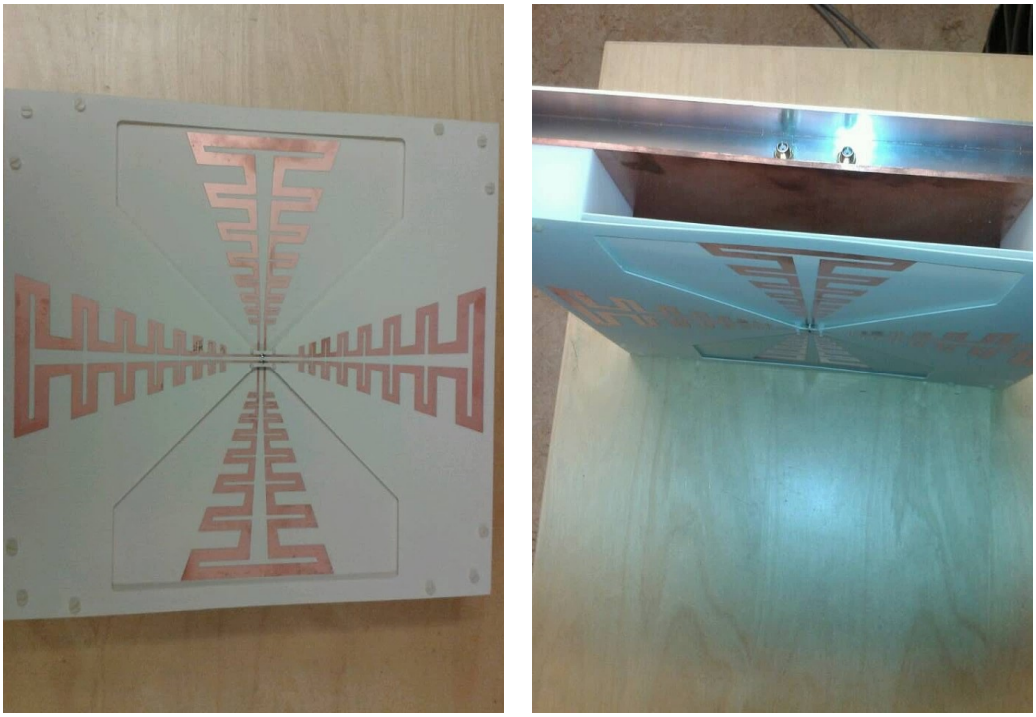

(a) Front view (b) Side view

Figure 3.10: The manufactured antenna

4

Measurement

This chapter first describe principles of two chambers - the anechoic chamber and the reverberation chamber - used in the measurement. Then the detailed procedures for the measurement of radiation pattern, radiation efficiency and S parameters are elaborated.

4.1 Antenna Measurement

After finishing the design and simulation of the antenna, it should be measured in the lab to see whether the performance of the antenna is agreement with the simulated results. Usually there are some differences between the simulation and the measurement.

The differences could result from the inaccuracy of the simulation in CST. In this design project, time domain solver is used in the simulation. There is simulation error since the meshes in the simulation could not be infinite. The denser are the meshes, the more accurate the result is. However, the time of the simulation will increase with the number of meshes. It's important to strike a careful balance between the accuracy and the simulation time. The equipments for the antenna test are not perfect and therefore the measurement results are not highly accurate. The inaccuracy of the measurement also contributes to the disagreement between the simulation and the measurement. The higher is the resolution of the equipment, the more accurate result it gives, as long as measurement is carried out in the right way.

If the simulation and the measurement are performed in the right way with properly chosen parameters, and the two results agree well with each other, the design is successful although both the simulation and the measurement are not perfectly accurate.

In this design project, two chambers, i.e. the anechoic chamber and the reverberation chamber are used for the antenna measurement, for simulating different environments.

4.1.1 Anechoic chamber

The anechoic chamber (AC) is a shielded room whose walls, ceiling and floor are covered with materials that absorb RF waves so that there is no reflection in the chamber. It simulates the free space environment. It is typically used for measuring radiation patterns of an antenna, electromagnetic compatibility and radar cross section, etc.

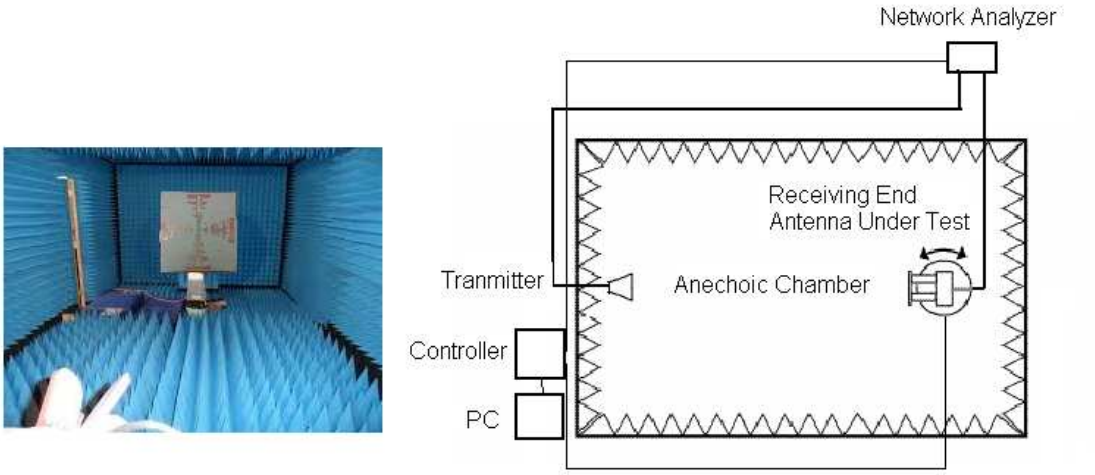

Figure 4.1: Antenna measurement in the anechoic chamber

A transmitting antenna is located at one side of the AC. The antenna under test (AUT) is located at the the other side of it facing the transmitting antenna (TA). Both the TA and the AUT are connected to the network analyzer through cables. A computer with profession software outside the chamber controls measurement procedure, e.g. the horizontal and vertical position, sweeping angle and speed of the AUT, and displays the measurement results.

4.1.2 Reverberation chamber

The reverberation chamber (RC) is a resonant, three dimensional cavity with cubic or rectangular form.

It supports a set of resonant modes that are stirred by moveable objects (mode-stirrers) inside the cavity. Thereby, different, independent field distributions are generated. The independent field distributions all together represent a statistically isotropic field, i.e. the test object will receive signals from all directions in space, and therefor a multipath environment, similar to real urban and indoor environments with no line-of sight to the base station, is created.

The RC provides an artificial Rayleigh fading environment. Antennas inside the RC experience Rayleigh fading and the measurements of embedded radiation efficiency and

diversity gains are made possible in the RC. The principle of operation of the chamber is elaborated in [55].

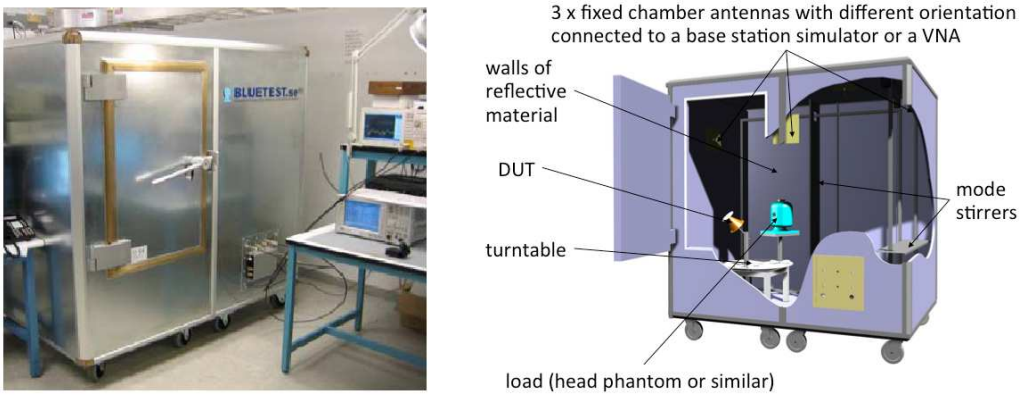

Figure 4.2: The reverberation chamber in Chalmers

4.2 Measurement of Radiation Pattern and Probability of Detection

The radiation pattern is measured in the AC. First connect the Eleven antenna to the receiving tower, facing the TA. The Eleven antenna is the AUT in Fig. 4.1. The AUT is set at the same vertical level as that of the TA and the elevation angle is set to zero before starting the measurement.

The far-field function (also the radiation pattern) described in eq. (2.27) is not possible to be measured in the AC since there is strong singular behaviour close to the polar point and the accuracy will be severely deteriorated due to the singularity. To obtain the radiation pattern, we measure the co-polar and cross-polar far-field function instead and form the real far-field according to eq. (2.30).

Both the co-polar radiation pattern and the cross-polar radiation are measured for every 5^o in the horizontal direction for all 360^o (one round) and every 15^o in the vertical direction. The co-polar radiation pattern is measure from -90^o to 90^o (half round) and the cross-polar radiation pattern is measured from -45^o to 90^o in the vertical direction. It's not necessary to measure the cross-polar pattern as many as the co-polar pattern, since what matters most is the co-polar pattern. Then, a two dimensional interpolation is implemented in matlab to retrieve the full far-field function for the total radiation pattern. The probability of detection as a function of frequency is obtained by employing the *ViRM-Lab* program [51] to process the far-field function.

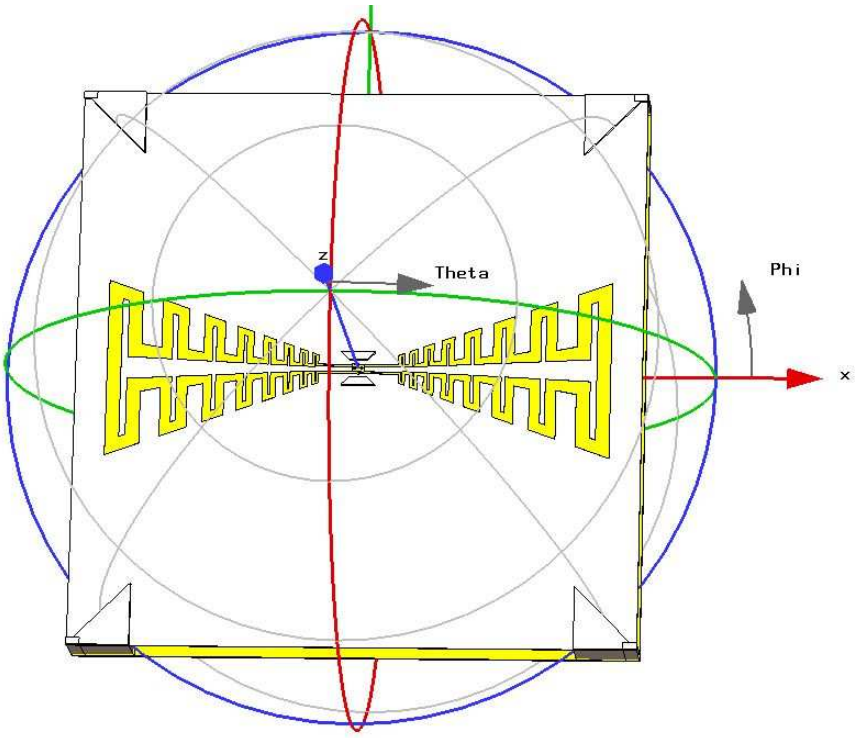

Figure 4.3: Illustration of the elevation angel (*Theta*) and horizontal angel (*Phi*) in CST. The antenna shown in the figure is the low branch with supporting structures.

4.3 Measurement of Radiation Efficiency

The radiation efficiency is measured in the reverberation chamber. To calibrate the reverberation chamber, a reference antenna (disk-cone antenna) with known radiation efficiency is measured in the chamber first. Then a correction parameter that quantifies the difference between the measured radiation efficiency in the chamber and the accurate radiation efficiency of the reference antenna is obtained. The measured radiation efficiency of the AUT is made accurate by compromising for this correction parameter afterwards.

4.4 Measurement of S Parameters

The S parameters of the antenna are measured with the vector network analyzer (VNA) Agilent E5071C . Before the measurement, the the ports in the VNA are calibrated with a quadrature hybrid so that the S_{11} read from the VNA are lower than $-20\ dB$ when connected with the hybrid.

Ideally the measurement should be taken in the anechoic chamber, since the reflection from the environment back to the antenna will influence the S parameters. However,

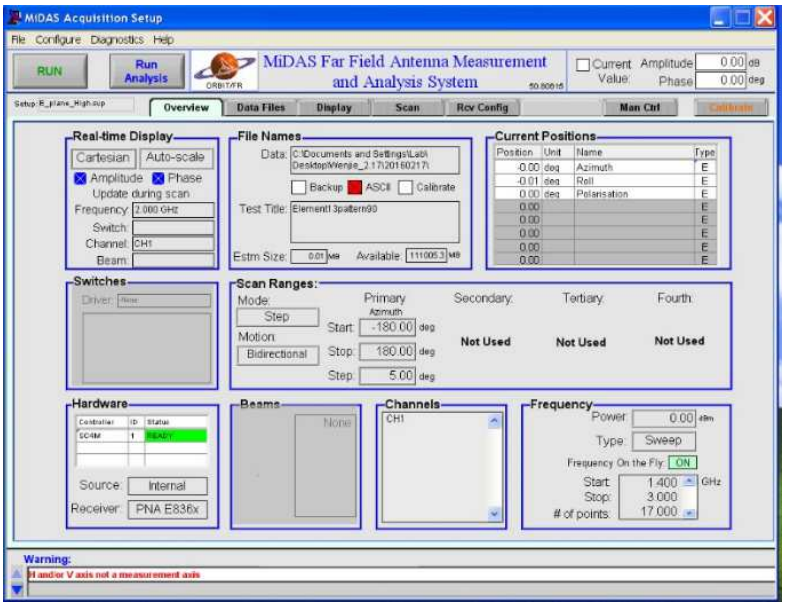

Figure 4.4: The software *MiDAS* for controlling the measurement in the anechoic chamber

Figure 4.5: The disk-cone antenna as reference in the reverberation chamber

due to the limitation in the laboratory, it can only be measured in the room. Since the antenna is facing the ceiling and the ceiling is high enough, the degradation on S parameters is negligible.

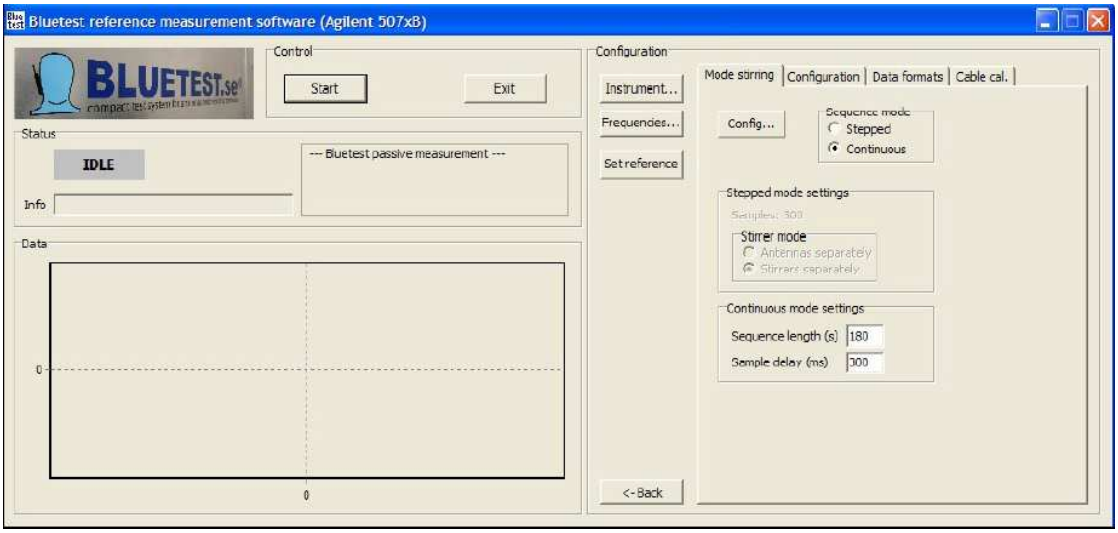

Figure 4.6: The software from Bluetest company for the radiation efficiency measurement

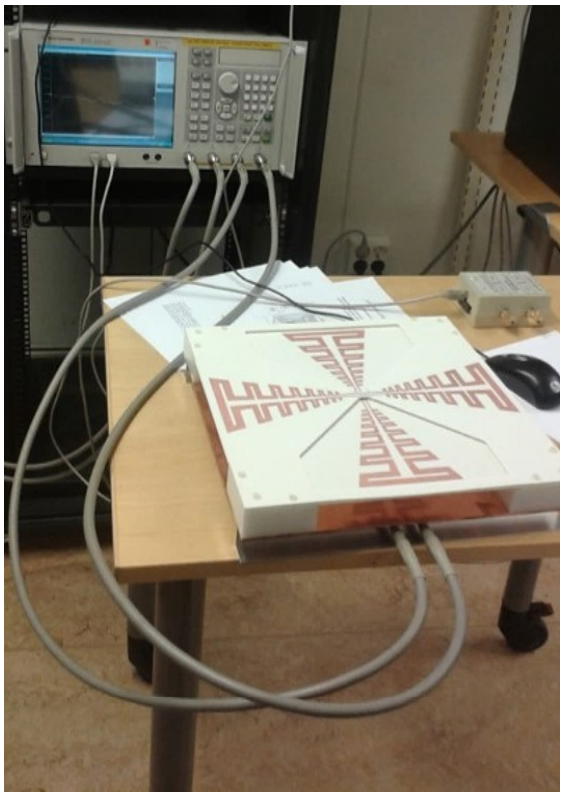

Figure 4.7: The measurement of S parameters with Agilent E5071C

5

Results and Discussion

This chapter presents the results from the simulation in CST and the measurement in the anechoic chamber and the reverberation chamber. The simulated results and the measured results are compared and contrasted. The reasons for the differences between the simulation and the measurements are analyzed.

5.1 S Parameters

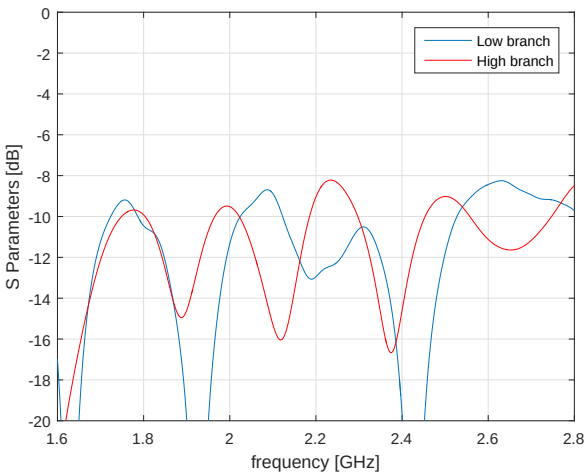

Figure 5.1: S parameters from simulation in CST

In the measurement of the S parameters for the low branch, the two ports (port 3 and port 4) for the high branch are terminated and the reflection from each single port

and the transmission between ports are measured. The real reflection from the port is the measured reflection subtracts the transmission between ports. The reflection in the high branch is obtained similarly.

It can be seen in figure 5.2 that the real reflection coefficient of the low branch is lower than -8 dB for the whole frequency range, which is in a good agreement with the simulation. The shape of S_{11} and S_{22} also matches well. For the high branch, the real reflection coefficient is below -8 dB for frequency ranging from 1.6 to 2.6 GHz. In the 2.6 to 2.8 GHz, it's less than -6 dB. The reason for this degradation is due to the imperfection of the manufacture.

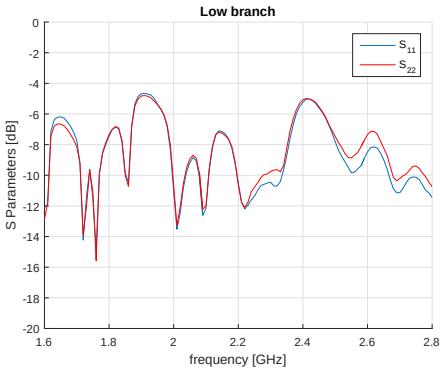

(a) Total reflection detected

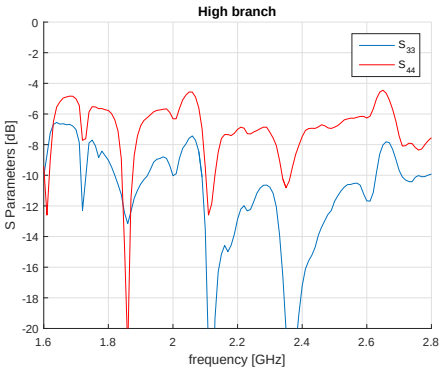

(b) Total reflection detected

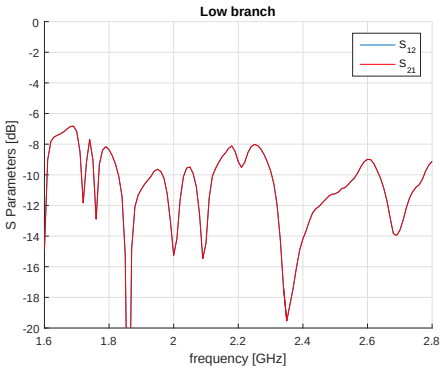

(c) Transmission between ports

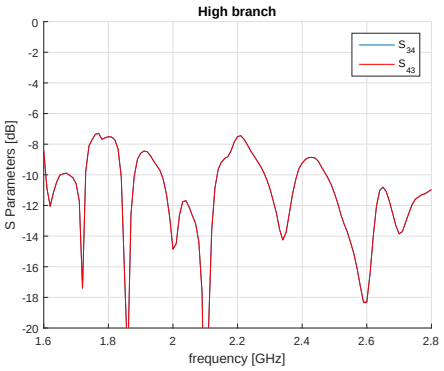

(d) Transmission between ports

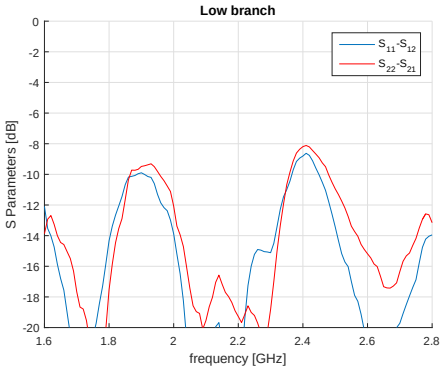

(e) Real reflection coefficients

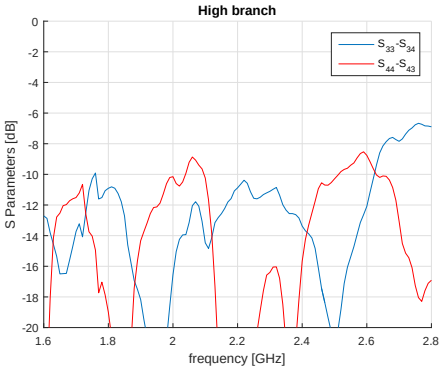

(f) Real reflection coefficients

Figure 5.2: S parameters from measurement

5.2 Total Embedded Radiation Efficiency

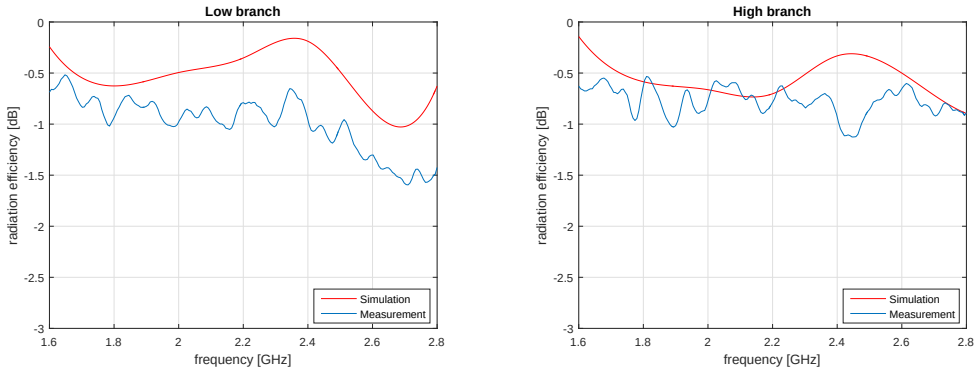

Figure 5.3: Total embedded radiation efficiency

The total radiation efficiency of both the high branch and the low branch is generally above -1 dB for the majority frequency range. For the low branch, there is a minor reduction in the total radiation efficiency in 2.6 to 2.8 GHz. The trend of the measured total radiation efficiency matches well with the simulated curve.

5.3 Radiation patterns

In the measurement setting, the low branch of the antenna is oriented along y-axis and the high branch is along x-axis. The radiation patterns of the low branch and the high branch in $\phi = 0$ and $\phi = 90^o$ planes for $f = 1.6GHz$, $f = 2.2GHz$ and $f = 2.8GHz$ are plotted in figure 5.4, 5.5 and 5.6, respectively.

It can be seen that the simulated curves are in good agreement with the measured curves. The measured radiation pattern is obtained by measuring the far-field functions with an step of $\Delta\phi = 15^o$ and $\Delta\theta = 5^o$ for both of the two orthogonal polarizations, and then interpolate the data in matlab so that the step in both directions becomes 1^o.

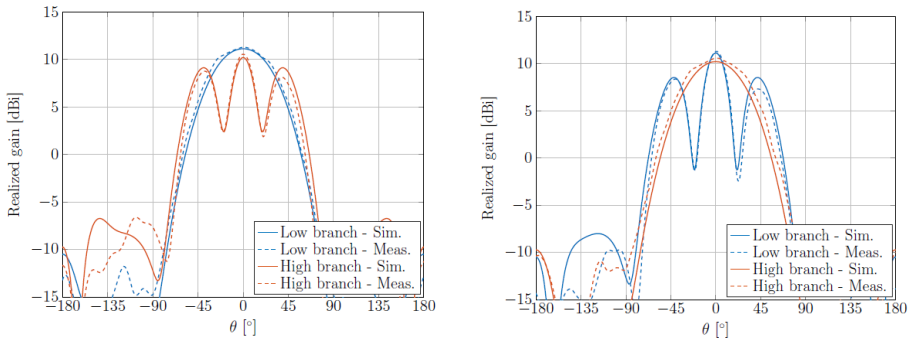

(a) $\phi = 0$ plane (b) $\phi = 90^0$ plane

Figure 5.4: Simulated and measured radiation patterns at 1.6 GHz

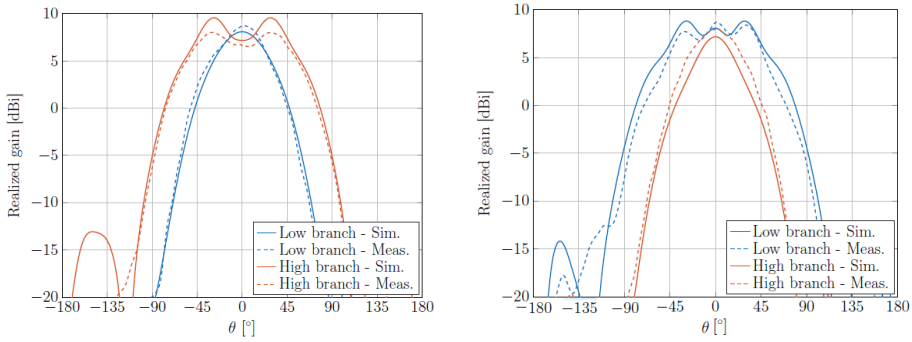

(a) $\phi = 0$ plane (b) $\phi = 90^0$ plane

Figure 5.5: Simulated and measured radiation patterns at 2.2 GHz

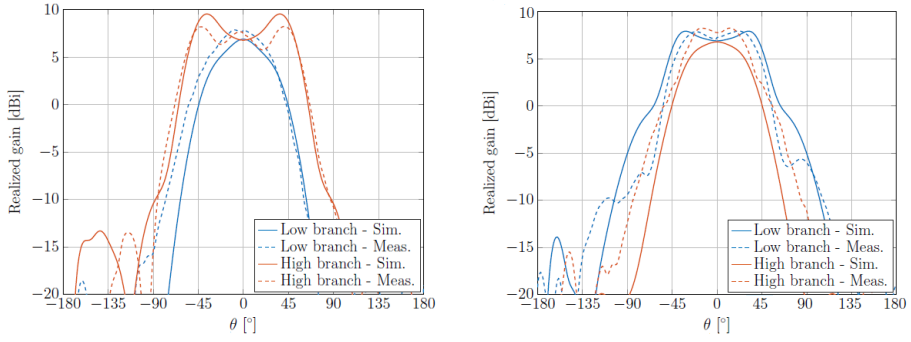

(a) $\phi = 0$ plane (b) $\phi = 90^0$ plane

Figure 5.6: Simulated and measured radiation patterns at 2.8 GHz

5.4 Probability of Detection

Figure 5.7 and 5.8 illustrate the relationship between the required average receiving power over the threshold (P_{av}/P_t) and the probability of detection for frequency ranging from 1.6 GHz to 2.8 GHz sampled at 7 equal distance frequency points under RIMP and RLOS environment, respectively. It can be seen that for both of the two environments, to achieve a higher probability of detection, more receiving power is needed; for a specific level of detection probability, the require receiving power of two streams zero forcing is higher than that of one stream MRC.

Figure 5.9 shows the required receiving power over the threshold for 95% probability of detection over the whole frequency range. It can be seen that in the RIMP environment, the variation of P_{av}/P_t is very small, approximately within 1 dB, whereas under RLOS environment, it's about 3 dB for two streams zero forcing. The reason for this difference is that in the RIMP environment, the distribution of angle-of-arrival (AoA) of the incoming waves is uniform and the polarization of the waves is balanced.

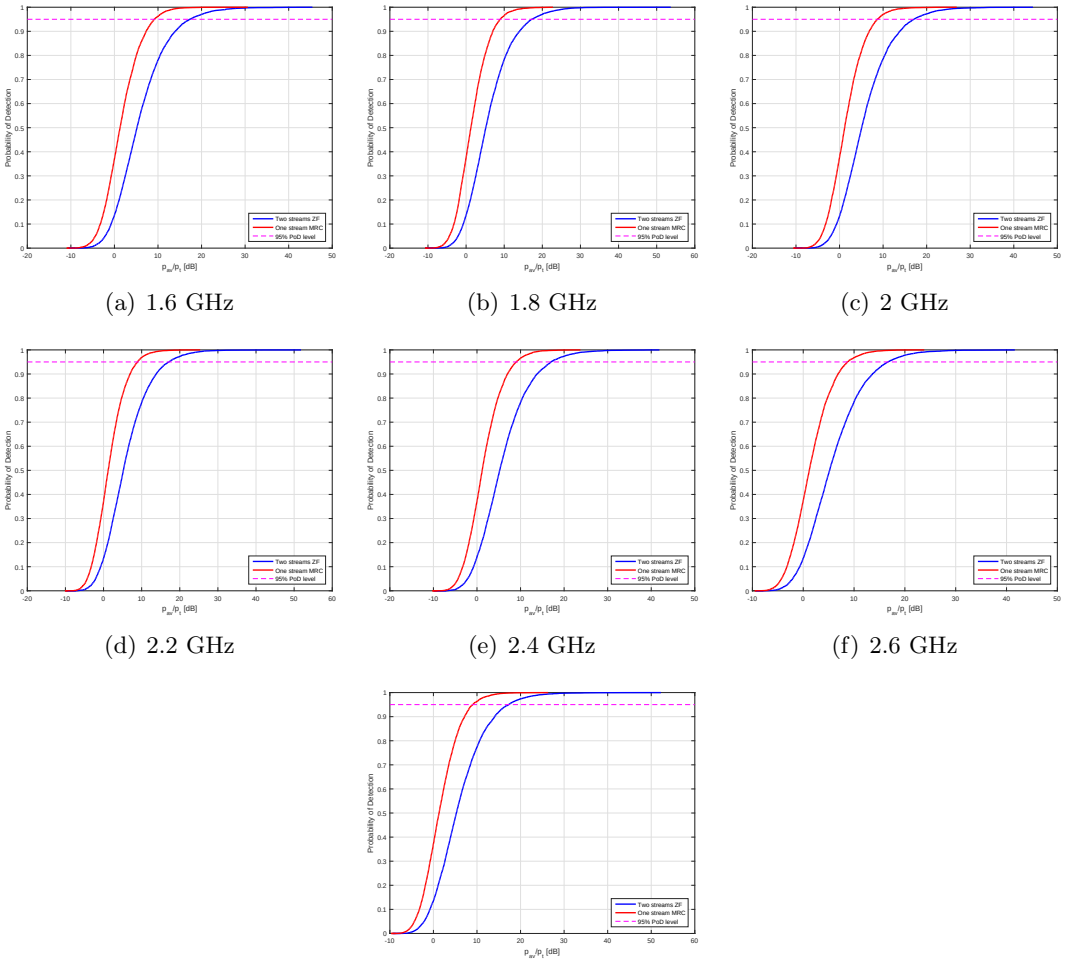

(a) 1.6 GHz (b) 1.8 GHz (c) 2 GHz

(d) 2.2 GHz (e) 2.4 GHz (f) 2.6 GHz

(g) 2.8 GHz

Figure 5.7: Probability of Detection in RIMP for Several Frequencies

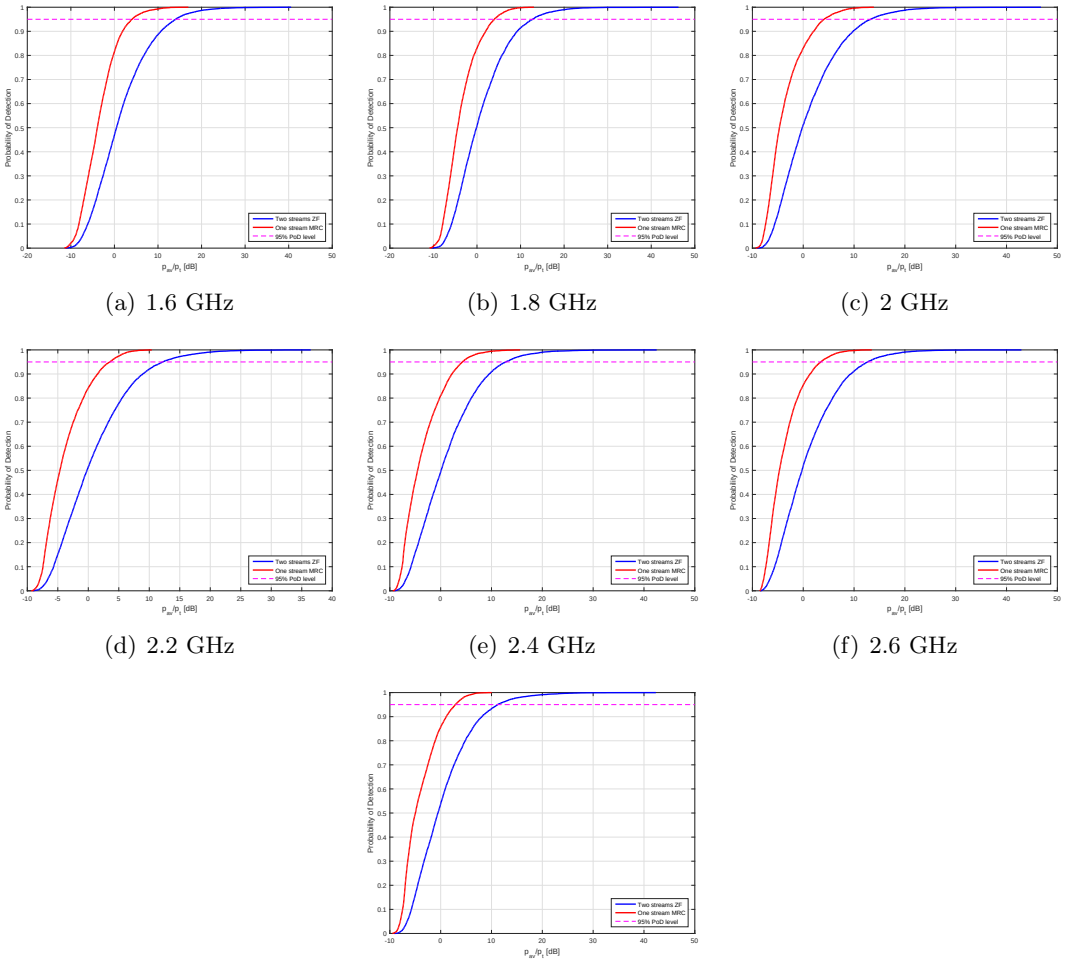

(a) 1.6 GHz (b) 1.8 GHz (c) 2 GHz

(d) 2.2 GHz (e) 2.4 GHz (f) 2.6 GHz

(g) 2.8 GHz

Figure 5.8: Probability of Detection in RLOS for Several Frequencies

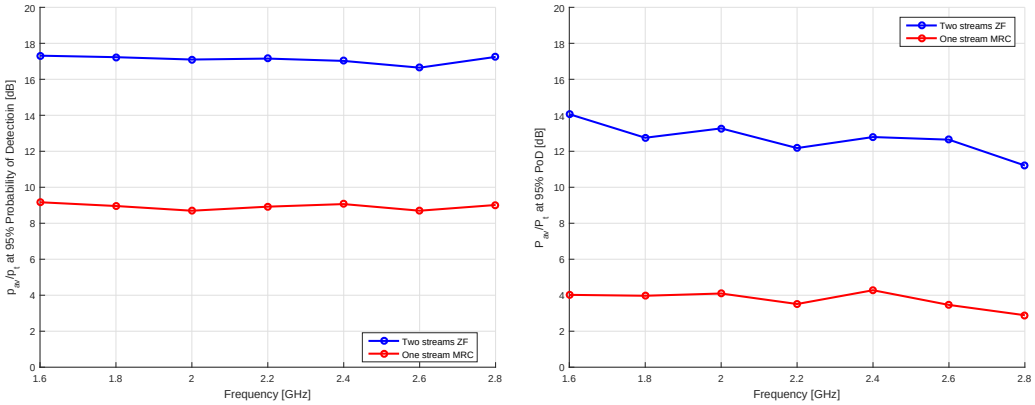

(a) RIMP (b) RLOS

Figure 5.9: Required p_{av}/p_t for 95% PoD Level in RIMP and RLOS as a Function of Frequency

5.5 Coverage pattern

The coverage pattern of the antenna on the beginning frequency, center frequency and ending frequency under the Random-LOS environment is plotted in figure 5.10. It can be seen that it works well in the desired 120^o window in θ direction and ϕ direction.

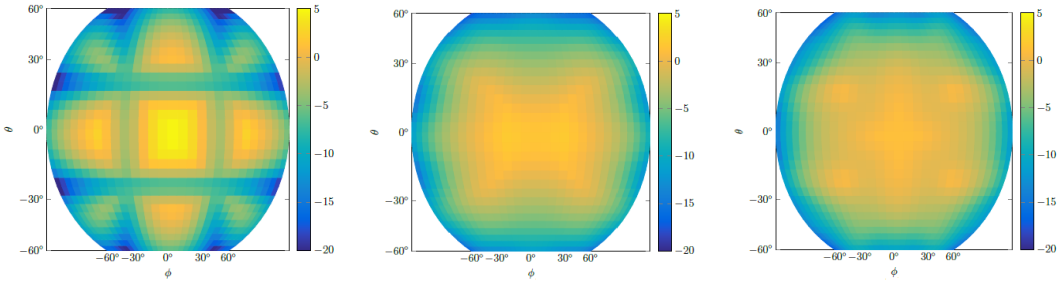

(a) 1.6 GHz (b) 2.2 GHz (c) 2.8 GHz

Figure 5.10: two port antenna 2-bitstream MIMO coverage pattern in RLOS

6

Conclusion

A planar eleven antenna for wideband MIMO micro-base station working on 1.6 GHz to 2.8 GHz is designed and the performance of antenna is optimized with genetic algorithms.

The reflection parameters, total embedded radiation efficiency, radiation patterns and coverage pattern are measured. The measurement is in good agreement with the simulation.

The planar shape reduces the manufacture complexity and therefore the cost. The antenna is suited for in-door wall-mounted applications.

Bibliography

[1] P. Hall, E. Dordrecht, The Square Kilometre Array: An Engineering Perspective, 2005.

[2] A. Niell, A. Whitney, B. Petrachenko, W. Schluter, N. Vandenberg, H. Hase, Y. Koyama, C. Ma, H. Schuh, G. Tuccari, VLBI2010: Current and future requirements for geodetic VLBI systems 2005, 2005.

[3] R. Olsson, P.-S. Kildal, S. Weinreb, The eleven antenna: a compact low-profile decade bandwidth dual polarized feed for reflector antennas, Antennas and Propagation, IEEE Transactions on 54 (2) (2006) 368–375.

[4] J. Yang, X. Chen, N. Wadefalk, P.-S. Kildal, Design and realization of a linearly polarized eleven feed for 1-10 ghz, Antennas and Wireless Propagation Letters, IEEE 8 (2009) 64–68.

[5] J. Yang, D. Nyberg, J. Yin, Impedance matrix of a folded dipole pair under eleven configuration, Microwaves, Antennas Propagation, IET 4 (6) (2010) 697–703.

[6] J. Yang, On conditions for constant radiation characteristics for log-periodic array antennas, Antennas and Propagation, IEEE Transactions on 58 (5) (2010) 1521–1526.

[7] J. Yang, P.-S. Kildal, Optimization of reflection coefficient of large log-periodic array by computing only a small part of it, Antennas and Propagation, IEEE Transactions on 59 (6) (2011) 1790–1797.

[8] J. Yang, M. Pantaleev, P.-S. Kildal, B. Klein, Y. Karandikar, L. Helldner, N. Wadefalk, C. Beaudoin, Cryogenic 2-13 ghz eleven feed for reflector antennas in future wideband radio telescopes, Antennas and Propagation, IEEE Transactions on 59 (6) (2011) 1918–1934.

[9] J. Yang, M. Panteleev, T. Ekebrand, P.-S. Kildal, H. Raza, J. Yin, J. Jonsson, L. Helldner, A. Emrich, B. Klein, Development of the cryogenic 2-14 ghz eleven feed

system for vlbi2010, in: Antennas and Propagation (EUCAP), 2012 6th European Conference on, 2012, pp. 621–625.

[10] J. Yin, J. Aas, J. Yang, P. Kildal, Monopulse tracking performance of multi-port eleven antenna for use in satellite communications terminals, in: Antennas and Propagation, 2007. EuCAP 2007. The Second European Conference on, 2007, pp. 1–4.

[11] J. Yang, S. Pivnenko, T. Laitinen, J. Carlsson, X. Chen, Measurements of diversity gain and radiation efficiency of the eleven antenna by using different measurement techniques, in: Antennas and Propagation (EuCAP), 2010 Proceedings of the Fourth European Conference on, 2010, pp. 1–5.

[12] X. Chen, P.-S. Kildal, J. Carlsson, J. Yang, Comparison of ergodic capacities from wideband mimo antenna measurements in reverberation chamber and anechoic chamber, Antennas and Wireless Propagation Letters, IEEE 10 (2011) 446–449.

[13] D. K. Cheng, Field and Wave Electromagnetics, 2nd Edition, Addison-Wesley Publishing Company, Inc., 1989.

[14] J. D. Kraus, Electromagnetics, 3rd Edition, McGraw-Hill, New York, USA, 1984.

[15] J. D. Jackson, Classical Electrodynamics, 3rd Edition, John Wiley & Sons, Inc., New Jersey, USA, 1991.

[16] D. Pozar, Microwave Engineering, 4th Edition, John Wiley & Sons, Inc., New York, NY, USA, 2011.

[17] R. E. Collin, Foundations for Microwave Engineering, 2nd Edition, John Wiley & Sons, Inc., New York, NY, USA, 2001.

[18] D. Pozar, Microwave and RF Design of Wireless Systems, 1st Edition, John Wiley & Sons, Inc., New York, NY, USA, 2001.

[19] P.-S. Kildal, Foundations of Antenna Engineering: A Unified Approach for Line-Of-Sight and Multipath, Kildal Antenn AB, 2015.

[20] C. A. Balanis, Antenna Theory, Analysis and Design, 3rd Edition, John Wiley & Sons, Inc., Hoboken, New Jersey, USA, 2005.

[21] Ieee standard definitions of terms for antennas, IEEE Std 145-1993 (1993) 1–32.

[22] J. G. Yin, J. Yang, M. Pantaleev, L. Helldner, The circular eleven antenna: A new decade-bandwidth feed for reflector antennas with high aperture efficiency, IEEE Transactions on Antennas and Propagation 61 (2013) 3976–3984.

[23] A. Yasin, J. Yang, T. Ostling, A compact dual-band feed for reflector antennas based on choke horn and circular eleven antenna, IEEE Transactions on Antennas and Propagation 57 (10) (2009) 3300–3302.

[24] J. Yin, W. Chen, J. Yang, Study on beamwidth flexibility of circular eleven feed for radio telescopes, in: EuCAP 2015, 2015.

[25] J. Yin, J. Yang, M. Pantaleev, L. Helldner, A circular eleven feed with significantly improved aperture efficiency over 1.3-14 ghz, in: Proceedings of 6th European Conference on Antennas and Propagation, EuCAP 2012. Prague, 26-30 March 2012, 2012, pp. 2353–2356.

[26] J. Yang, M. Pantaleev, B. Billade, M. Ivashina, T. Carozzi, L. Helldner, M. Dahlgren, A compact dual-polarized 4-port eleven feed with high sensitivity for reflectors over 0.35-1.05 ghz, IEEE Transactions on Antennas and Propagation 63 5955–5960.

[27] J. Yang, Periodicity of the input impedance of log-periodic array antennas, IET Microwaves, Antennas & Propagation 6 (2012) 1117–1122.

[28] X. Chen, P.-S. Kildal, J. Carlsson, J. Yang, Mrc diversity and mimo capacity evaluations of multi-port antennas using reverberation chamber and anechoic chamber, IEEE Transactions on Antennas and Propagation 61 (2013) 917–926.

[29] J. Yang, S. Pivnenko, P.-S. Kildal, Comparison of two decade bandwidth feeds for reflector antennas: Eleven antenna and quadridge horn, in: EuCAP 2010 Fourth European Conference on Antennas and Propagation, Barcelona, 12-16 April 2010, 2010.

[30] P.-S. Kildal, R. Olsson, J. Yang, Development of three models of the eleven antenna: A new decade bandwidth high performance feed for reflectors, in: Antennas and Propagation, 2006. EuCAP 2006. First European Conference on, 2006, pp. 1–6.

[31] J. Yang, M. Pantaleev, Truly conical eleven antenna: a new geometry for applications at high frequencies, in: 2016 IEEE AP-S International Symposium, Puerto Rico, , June 25-July 1, 2016, 2016.

[32] P.-S. Kildal, The hat feed: a dual-mode rear-radiating wave-guide antenna having low cross-polarization, IEEE Transactions on Antennas and Propagation.

[33] J. Yang, P.-S. Kildal, Fdtd design of a chinese hat feed for shallow mm-wave reflector antennas, in: IEEE AP-S International Symposium, Atlanta, June, 1998., 1998.

[34] M. Denstedt, T. Östling, J. Yang, P.-S. Kildal, Tripling bandwidth of hat feed by genetic algorithm optimization, in: IEEE AP-S 2007 in Hawai, 10-15 June 2007, 2007.

[35] W. Wei, J. Yang, T. Ostling, T. Schafer, New hat feed for reflector antennas realised without dielectrics for reducing manufacturing cost and improving reflection coefficient, IET Microwaves Antennas & Propagation 5 (2011) 837–843.

[36] E. G. Geterud, J. Yang, T. Östling, P. Bergmark, Design and optimization of compact wideband hat-fed reflector antenna for satellite communications, IEEE Transactions on Antennas and Propagation 61 (2013) 125–133.

[37] E. G. Geterud, J. Yang, T. Östling, Wide band hat-fed reflector antenna for satellite communications, in: Proceedings of the 5th European Conference on Antennas and Propagation, EUCAP 2011. Rome, 11-15 April 2011, 2011, pp. 754–757.

[38] E. G. Geterud, J. Yang, T. Östling, Radome design for hat-fed reflector antenna, in: Proceedings of 6th European Conference on Antennas and Propagation, EuCAP 2012. Prague, 26-30 March 2012, 2012, pp. 2985–2988.

[39] J. Yang, A. Kishk, A novel low-profile compact directional ultra-wideband antenna: the self-grounded bow-tie antenna, IEEE Transactions on Antennas and Propagation 60 (2012) 1214–1220.

[40] Y. Yu, J. Yang, T. McKelvey, B. Stoew, Compact uwb indoor and through-wall radar with precise ranging and tracking, International Journal of Antennas and Propagation 2012 (2012) Article ID 678590.

[41] H. Raza, A. Hussain, J. Yang, P.-S. Kildal, Wideband compact 4-port dual polarized self-grounded bowtie antenna, IEEE Transactions on Antennas and Propagation 62 (2014) 4468–4473.

[42] J. Yang, A. Kishk, The self-grounded bow-tie antenna, in: 2011 IEEE International Symposium on Antennas and Propagation, Spokane, USA, 3-8 July, 2011, 2011, pp. 1452–1455.

[43] S. Abtahi, J. Yang, S. Kidborg, A new compact multiband antenna for stroke diagnosis system over 0.5–3 ghz, Microwave and Optical Technology Letters 54 (2012) 2342–2346.

[44] S. Mansouri Moghaddam, A. A. Glazunov, J. Yang, M. Gustafsson, P.-S. Kildal, Comparison of 2-bitstream polarization-mimo performance of 2 and 4-port bowtie antennas for lte in random-los, in: International Symposium on Antennas and Propagation (ISAP), Ieee, 2015.

[45] M. P. Jian Yang, Jonas Flygare, B. Billade, Development of quadruple-ridge flared horn with spline-defined profile for band b of the wide band single pixel feed (wbspf) advanced instrumentation programme for ska, in: 2016 IEEE AP-S International Symposium, Puerto Rico, June 25-July 1, 2016, 2016.

[46] A. Paulraj, R. Nabar, D. Gore, Introduction to Space-Time Wireless Communications, 1st Edition, Cambridge University Press, New York, NY, USA, 2008.

[47] X. Chen, P.-S. Kildal, M. Gustafsson, Characterization of implemented algorithm for mimo spatial multiplexing in reverberation chamber, Antennas and Propagation, IEEE Transactions on 61 (8) (2013) 4400–4404.

[48] P.-S. Kildal, J. Carlsson, New approach to ota testing: Rimp and pure-los as reference environments & a hypothesis [elektronisk resurs], 7th European Conference on Antennas and Propagation, EuCAP 2013, Gothenburg, Sweden, 8-12 April 2013 s. 315-318.

[49] P.-S. Kildal, Rethinking the wireless channel for ota testing and network optimization by including user statistics: Rimp, pure-los, throughput and detection probability, in: 2013 Proceedings of The International Symposium on Antennas and Propagation (ISAP), Vols 1 and 2.

[50] P.-S. Kildal, X. Chen, M. Gustafsson, Z. Shen, Mimo characterization on system level of 5g microbase stations subject to randomness in los, Access, IEEE 2 (2014) 1064–1077.

[51] U. Carlberg, J. Carlsson, A. Hussain, P.-S. Kildal, Ray based multipath simulation tool for studying convergence and estimating ergodic capacity and diversity gain for antennas with given far-field functions, in: ICECom, 2010 Conference Proceedings, 2010, pp. 1–4.

[52] P.-S. Kildal, Equivalent circuits of receive antennas in signal processing arrays, Microwave and Optical Technology Letters 21 (1999) 244–246.

[53] P.-S. Kildal, A. Hussain, X. Chen, C. Orlenius, A. Skarbratt, J. Asberg, T. Svensson, T. Eriksson, Threshold receiver model for throughput of wireless devices with mimo and frequency diversity measured in reverberation chamber, Antennas and Wireless Propagation Letters, IEEE 10 (2011) 1201–1204.

[54] A. Goldsmith, Wireless Communications, Cambridge University Press, New York, NY, USA, 2005.

[55] K. Rosengren, P.-S. Kildal, Study of distributions of modes and plane waves in reverberation chambers for the characterization of antennas in a multipath environment, Microwave and Optical Technology Letters 30 (2001) 386–391.